Polypharmacological Modulation of Atrial Fibrillation: Rational Design, Synthesis, and Evaluation of Novel Compounds Targeting $Na_V1.5$, $K_V1.5$, and K_2P Channels

Lorena Camargo-Ayala[1,†], Mauricio Bedoya[2,3,†], Albert Dasí[4†], Merten Prüser[5,6,7†], Luis Prent-Peñaloza[8], Francisco Adasme-Carreño[2,3], Aytug K Kiper[9], Susanne Rinné[9], Paola Andrea Camargo-Ayala[10], Paula A Peña-Martínez[11,12], Alfonso Bueno-Orovio[4], Diego Varela[13,14], Felix Wiedmann[5,6,7], José C. E. Márquez-Montesinos[15], Constanze Schmidt[5,6,7*], Blanca Rodriguez[4*], Ursula Ravens[16,17*], Niels Decher[9]*, Margarita Gutiérrez[18,*], and Wendy González[13,15*]

[1] Doctorado en Ciencias Mención I + D de Productos Bioactivos, Instituto de Química de Recursos Naturales, Laboratorio de Síntesis Orgánica, Universidad de Talca, Casilla 747, Talca 3460000, Chile. [2] Centro de Investigación de Estudios Avanzados del Maule (CIEAM), Vicerrectoría de Investigación y Postgrado, Universidad Católica del Maule, Talca 3480112, Chile. [3]Laboratorio de Bioinformática y Química Computacional (LBQC), Departamento de Medicina Traslacional, Facultad de Medicina, Universidad Católica del Maule, Talca 3480112, Chile. [4]Department of Computer Science, British Heart Foundation Centre of Research Excellence, University of Oxford, Oxford, UK. [5]Department of Cardiology, University of Heidelberg, Heidelberg, Germany. [6]DZHK (German Center for Cardiovascular Research), partner site Heidelberg /Mannheim, University of Heidelberg, Heidelberg,Germany. [7]HCR, Heidelberg Center for Heart

Rhythm Disorders, University of Heidelberg, Heidelberg, Germany. [8]Departamento de Ciencias Químicas, Facultad de Ciencias Exactas, Universidad Andrés Bello, Quillota 980, Viña del Mar, Chile. [9]Institute for Physiology and Pathophysiology, Philipps-University Marburg, Marburg, Germany. [10]Doctorado en Ciencias Biomédicas, Laboratorio de Patología Molecular, Departamento de Ciencias Básicas Biomédicas, Facultad de Ciencias de la Salud, Universidad de Talca, Talca 3460000, Chile. [11]Doctorado en Ciencias Agrarias, Facultad de Ciencias Agrarias, Universidad de Talca, Talca, Chile. [12]Laboratorio de Química Enológica, Facultad de Ciencias Agrarias, Universidad de Talca, Talca, Chile [13]Millennium Nucleus of Ion Channels-Associated Diseases (MiNICAD), Santiago, Chile. [14]Program of Physiology and Biophysics, Institute of Biomedical Sciences, Faculty of Medicine, Universidad de Chile, Santiago, Chile. [15]Centro de Bioinformática, Simulación y Modelado (CBSM), Universidad de Talca, Casilla 747, Talca 3460000, Chile. [16]German Atrial Fibrillation Competence NETwork (AFNET), Germany. [17]Institute of Experimental Cardiovascular Medicine, University Heart Center Freiburg – Bad Krozingen, Medical Center – University of Freiburg and Faculty of Medicine, Freiburg, Germany. [18]Laboratorio Síntesis Orgánica y Actividad Biológica (LSO-Act-Bio), Instituto de Química de Recursos Naturales, Universidad de Talca, Casilla 747, Talca 3460000, Chile.

*Corresponding author: Constanze Schmidt. Department of Cardiology, University of Heidelberg, Heidelberg, Germany. DZHK (German Center for Cardiovascular Research), partner site Heidelberg /Mannheim, University of Heidelberg, Heidelberg, Germany. HCR, Heidelberg Center for Heart Rhythm Disorders, University of

Heidelberg, Heidelberg, Germany. Blanca Rodriguez, Department of Computer Science, British Heart Foundation Centre of Research Excellence, University of Oxford, Oxford, UK. Ursula Ravens, German Atrial Fibrillation Competence NETwork (AFNET), Germany. Department of Pharmacology, Technical University Dresden, Germany. Niels Decher, Institute for Physiology and Pathophysiology, Philipps-University Marburg, Marburg, Germany. Margarita Gutiérrez, Laboratorio Síntesis Orgánica y Actividad Biológica (LSO-Act-Bio), Instituto de Química de Recursos Naturales, Universidad de Talca, Casilla 747, Talca 3460000, Chile. Wendy González, Centro de Bioinformática, Simulación y Modelado (CBSM), Universidad de Talca, Casilla 747, Talca 3460000, Chile. E-mail address: constanze.schmidt@med.uni-heidelberg.de (CS), blanca.rodriguez@cs.ox.ac.uk (BR), ursula.ravens@uniklinik-freiburg.de (UR), decher@staff.uni-marburg.de (ND), mgutierrez@utalca.cl (MG), wgonzalez@utalca.cl (WG).

Abstract

During atrial fibrillation (AF), electrical remodeling occurs, involving ion channels like $Na_V1.5$, $K_V1.5$, and TASK-1. A promising AF treatment encompasses inhibiting these channels. In this study, acetamide compounds were designed based on the local anesthetic pharmacophore as potential $Na_V1.5$, $K_V1.5$, and TASK-1 inhibitors. Compound **6f** emerged as the most potent in the series, with IC_{50} values determined in *Xenopus* oocytes of approximately 0.3 µM in TASK-1, 81.5 µM in $K_V1.5$, and 21.2 µM in $Na_V1.5$. Unexpectedly, **6f** activated at 100 µM another cardiac K_2P channel (TASK-4) by about 40%. Next, we performed patch clamp experiments of human atrial cardiomyocytes from sinus rhythm (SR) or AF patients. In SR **6f** reduced action potential amplitude (indicating $Na_V1.5$ block) while in AF it increased action potential duration (APD), reflecting high affinity for TASK-1. Additionally, a hyperpolarization in resting membrane potential occurred in AF cardiomyocytes by **6f**, consistent with the TASK-4 activation we observed. In a mathematical whole-atria model, **6f** prolonged APD and tissue refractoriness, proving efficacious both for AF prevention and cardioversion. Favorable pharmacokinetic properties of **6f** *in silico*, including good absorption and low toxicity, as well as its lack of cytotoxicity in a hemolytic assay, suggest its potential as an AF treatment.

Key words: Atrial fibrillation; ion channels; K_2P channels; $K_V1.5$; $Na_V1.5$.

Introduction

The regular beating of the heart depends on the generation of action potentials that

trigger coordinated contractions. Each action potential (AP) is governed by the ordered opening and closing of plasmalemmal ion channels that produce a rapid depolarization and a slow repolarization. Alterations in these processes can lead to perturbation of the regular cardiac rhythm which presents as cardiac arrhythmias. Atrial fibrillation (AF) is the most common arrhythmia in clinical practice globally and is associated with a heightened risk of thromboembolic events, heart failure worsening, and more generally, cardiovascular morbidity and mortality [1,2]. It is estimated that at least 5 million new cases of AF will occur each year [3], and by 2030, more than 12 million cases are expected in the United States alone [4]. The rise in the incidence of AF has been linked to various factors such as the aging of the population, the prevalence of obesity, and improved survival after a first cardiovascular event [5].

One of the underlying causes of persistent AF is atrial remodeling, defined as any change in atrial function associated with structural or electrical factors [6,7]. Electrical remodeling is characterized by changes in ion channel expression and alterations in the function of various ion channels. The result of electrical remodeling is typically a shortened atrial action potential and a shortened atrial refractoriness, which, in turn, facilitates the maintenance and re-occurrence of AF by enhancing re-entry of triggering impulses ("AF begets AF") [7].

To reverse the AF-promoting effects of electrical remodeling, ion channels in the atrium are essential therapeutic targets. Voltage-dependent potassium channels $K_V1.5$ are preferentially expressed in human atria but not in ventricles [8,9], and they are responsible for the ultrafast potassium outflow current (I_{Kur}). $K_V1.5$ regulates the

cellular repolarization, shaping the APD [10]. Therefore, I_{Kur} channel blockers are expected to selectively prolong the atrial effective refractory period without inducing proarrhythmic effects in the ventricles [9], making $K_V1.5$ a promising pharmacological target for the treatment of AF [11–14]. Hence, numerous I_{Kur} blockers, acting through different mechanisms, have been developed. These mechanisms include 1) binding to the internal vestibule of the channel, thus interfering with the closing of the activation gate [15], 2) block of open channels with drug access from the intracellular side and positioning at the internal cavity of the pore [9], or 3) simultaneous binding at the central cavity (CC) and the side pockets (SP) [16,17].

Other potassium channels strongly contributing to the atrial AP include the two-pore domain (K_{2P}) channel TASK-1 [18], which, in the human heart, is predominantly expressed in the atria [18–20]. In patients with AF, an increased expression level of this channel has been shown to speed up repolarization and induce AP shortening [20–22]. Additionally, the current density of TASK-1 in human atrial cardiomyocytes isolated from patients with AF is three times higher than in patients in sinus rhythm [19]. Blocking TASK-1 channels is associated with normalization of the atrial AP-duration, making them an attractive pharmacological target for a new antiarrhythmic strategy [13,18–20,22–25]. Moreover, it has been reported that $K_V1.5$ blockers used against AF can also inhibit TASK-1 channels [26], suggesting that a polypharmacological strategy targeting both $K_V1.5$ and TASK-1 could potentiate the clinical efficacy of these drugs.

Another channel that plays an essential role in the physiology of the heart is the voltage-dependent sodium channel $Na_V1.5$ [26,27], which is responsible for the

upstroke (the initial depolarizing phase) of the AP [28]. An increased peak sodium current mediated by the $Na_V1.5$ channel has been described as a potential cause for increased atrial excitability and AF [29]. Although it is present in both atria and ventricles, its differential biophysical properties in the atria make it an attractive pharmacological target for the treatment of AF [8,10,30]. In fact, class I antiarrhythmic drugs (those targeting $Na_V1.5$ channel) have long been used for rhythm control in clinical practice, thus highlighting the functional relevance of $Na_V1.5$ channel inhibition in AF therapy [31].

Current evidence suggests that the development of effective and safe antiarrhythmic drugs remains an unmet clinical need [32], as the available therapeutic options are limited by poor efficacy and adverse effects [13,20]. Moreover, pure I_{Kur} channel blockade may not be sufficient to suppress AF [9]. Therefore, it has been proposed that multichannel blockers could represent better strategies for treating AF [32]. For example, compounds with the capacity to block $K_V1.5$ channels and simultaneously blocking $Na_V1.5$ channels can generate a synergistic anti-AF effect, without giving rise to ventricular proarrhythmic adverse effect [32–34]. Similarly, it has been suggested that the inhibition of I_{Na} and combined multi K^+-current block produces synergistic effects with regard to normalization of the shortened AP in patients with AF [33].

Local anesthetic (LA) compounds, such as lidocaine, ropivacaine, and bupivacaine **(Figure 1)**, are used as antiarrhythmics drugs in clinical practice [35,36] and were shown to have multiple mechanisms of action [36]. Ropivacaine and bupivacaine block

$Na_V1.5$, TASK-1 and $K_V1.5$ channels. In contrast, lidocaine blocks both $Na_V1.5$ and TASK-1 [37–42]. The primary purpose of this study is to obtain, through rational design and organic synthesis, new molecules based on the chemical common features of LA, capable of inhibiting the function of ion channels present in the atria, specifically $Na_V1.5$, TASK-1, and $K_V1.5$.

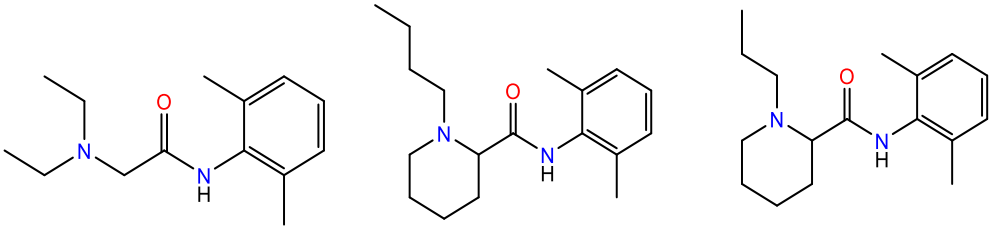

Figure 1. Structures of LA compounds that block $K_V1.5$, TASK-1 and/or $Na_V1.5$ channels. From the right to the left of the compounds are shown the aromatic ring, an intermediate amide linker and a hydrophilic domain.

Results and discussion

In-silico design: molecular docking

Ligand design

The pharmacophore of LA typically includes several key features that are important for their activity, such as the presence of a hydrophobic domain or aromatic ring (mono, di, or tri-substituted), an intermediate amide linker, a hydrophilic domain (amine) **(Figure 1)**, and proton donor and acceptor groups capable of interacting with amino acid residues at binding site (BS). Based on three criteria: a) the common pharmacophore of LA used as antiarrhythmics (bupivacaine, ropivacaine, and lidocaine) that has been shown to block $K_V1.5$, TASK-1, and $Na_V1.5$ channels, b) their reported binding modes in these channels and c) viability of synthesis, we proposed a basic core for the candidate compounds **(Figure 2 A, B).**

Aromatic amines were selected to explore different numbers and types of substituents, including mono and disubstituted amines with electron donor and acceptor groups. Similarly, aliphatic amines were chosen to introduce variability in terms of chain extension and the presence of cyclic and acyclic chains. We then proposed two series of compounds, resulting in 30 compounds derived from bromoacetic acid **(Figure 2A)** and 30 compounds derived from (*S*)-2-bromo-propionic acid **(Figure 2B)**, making a total of 60 proposed compounds.

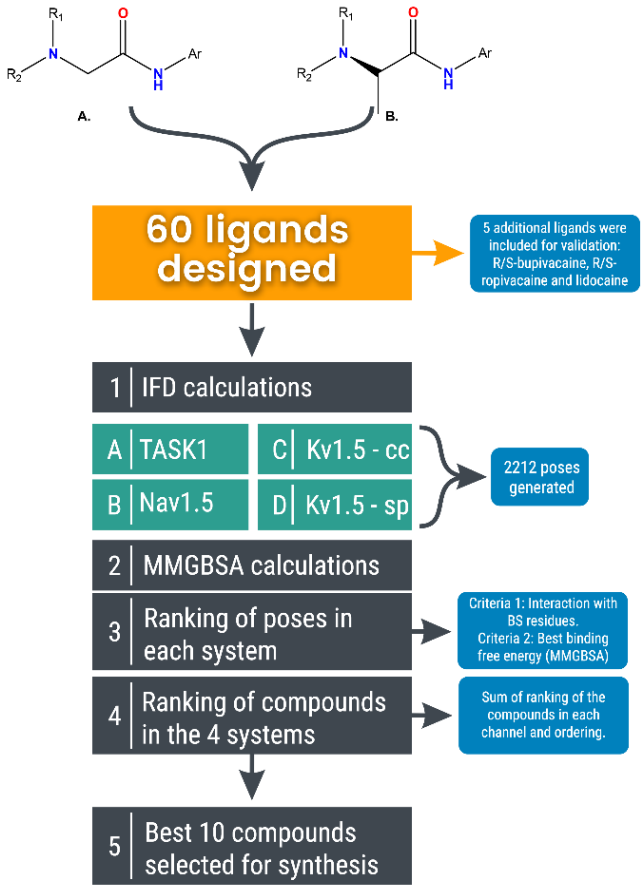

Figure 2. General scheme of design and selection of compounds for synthesis. A. Derivatives of bromoacetic acid. B. (*S*)-2-bromo-propionic acid derivatives.

Computational Analysis

Induced-fit docking (IFD) calculations were conducted for the 60 proposed candidates with each of the channels. These calculations aimed to analyze the most probable binding mode and the potential ligand-receptor interactions, using the BS references reported for LA-type blockers: lidocaine at $Na_V1.5$ [43], the enantiomers of bupivacaine in TASK-1 [44], and bupivacaine and ropivacaine in $K_V1.5$ [16]. After adequately preparing the ligands and the proteins, molecular docking calculations were executed for each of the proposed ligands, generating a maximum of 10 poses per ligand.

The IFD method employed the Glide and Prime modules incorporated in the Schrödinger

suite [45], utilizing the standard precision (SP) scoring function and obtaining a maximum of 10 poses *per* docking simulation. For the molecular docking calculations in TASK-1, a single protein lateral fenestration was explored due to the symmetrical nature of both subunits. The exploration of fenestration considered the BS residues reported for bupivacaine.

Similarly, in the case of $K_V1.5$, the residues reported as key in the binding of the LA bupivacaine and ropivacaine were considered. However, since interactions with LA have been documented in both the CC and SP of $K_V1.5$, separate molecular docking calculations were performed for each of these sites.

Regarding $Na_V1.5$, the analysis focused on the residues associated with lidocaine binding in its four domains. In total, approximately 550 poses were obtained for each system, resulting in a combined total of 2,212 poses **(**Step 1, **Figure 2)**. This accounts for a maximum of 10 poses per ligand, involving 60 designed compounds and an additional five compounds for validation (*R* and *S* bupivacaine, *R* and *S* ropivacaine and lidocaine) for each of the TASK-1, $Na_V1.5$, and $K_V1.5$ (CC and SP) channels.

Once the molecular docking results were acquired through the IFD protocol, binding free energy calculations were carried out to re-score and analyze the poses obtained for each channel **(**Step2, **Figure 2)**. These energy calculations utilized the Molecular Mechanics with Generalized Born and Surface Area (MM-GBSA) method, which is part of the Prime module in the Schrödinger suite. The MM-GBSA calculations is employed to estimate the binding free energy of small ligands to biological macromolecules. This estimation is based on molecular mechanics and implicit solvation approaches for the

receptor-ligand complex. Therefore, MM-GBSA calculations represent an intermediate approach in terms of precision and computational effort, falling between scoring empirical methods and perturbation methods [46].

Selection of the Best Ligands: Total Score and Location in the Ranking

Two criteria were integrated to rank the compounds and identify those with the most significant polypharmacological potential, namely, the highest activity across all three channels. The first criterion encompassed the interaction of the tested compounds with residues within the documented BS of LA in each channel. This criterion constituted the initial assumption that the studied compounds could share the reported LA BS due to the inclusion of the LA pharmacophore in the molecules design. The second criterion involved the determination of binding free energy using the IFD protocol, followed by the MM-GBSA method. This second criterion represented the secondary assumption that binding free energy might serve as an indicator to predict or estimate the potential affinities of the studied compounds.

In summary, we devised a methodology for ranking the compounds, which entailed identifying those with the highest number of interactions and optimal binding free energy values in each channel. This phase of the process is referred to as the "ranking of poses," as illustrated in Step 3, **Figure 2**.

Since multiple poses were obtained for each calculation from the docking results, this step involved selecting the best pose that satisfied the two aforementioned criteria for each compound. The binding free energy values and the maximum number of interactions detected were individually normalized. These normalized values were then

employed to arrange the poses, ensuring that the most favorable pose received the highest cumulative value. Subsequently, a "ranking of compounds" was executed *per* channel **(Table 1).**

Table 1. Ranking of the 25 compounds with the highest polypharmacological potential on TASK1, $K_V1.5$ and $Na_V1.5$ channels.

POSITION	NAME
1	6d
2	6f
3	7d
4	6a
5	7c
6	7a
7	6c
8	ropivacaine *S*
9	7b
10	bupivacaine *R*
11	6e
12	6b
13	6p
14	6x
15	7i
16	7w
17	7aa
18	7h
19	bupivacaine *S*
20	7x
21	7j
22	ropivacaine *R*
23	6z
24	7ab
25	6o

Analyzing the individual rankings, it is known for $K_V1.5$, that the *R/S* mixture of bupivacaine has an IC_{50} of 31 µM, whereas the *S* enantiomer of ropivacaine has an IC_{50} of 128.9 µM in oocytes for both compounds [16]. This finding is consistent with the ranking obtained for compounds in the $K_V1.5$ channel **(Table S1).** In the CC, *R/S* bupivacaine occupies positions 2 and 3, while *S*-ropivacaine occupies position 5.

However, in the case of $K_V1.5$ side-pockets **(Table S2)**, *S*-ropivacaine occupies position 12, and *R*/S-bupivacaine occupies positions 18 and 20. The effect in $K_V1.5$ is complex as the LA can bind in both sites. Nonetheless, in this scenario, the IC_{50} values are consistent with the optimal positions of *R/S*-bupivacaine in the CC.

The IC_{50} values for *R*/*S*-bupivacaine, *R*/*S*-ropivacaine and lidocaine in TASK-1 are quite similar; 12.1 μM, 17.6 μM and 53.8 μM, respectively [39]. In the compounds ranking for TASK-1, *R/S*-ropivacaine ranked 19th and 21st, *R/S*-bupivacaine ranked 33rd and 62nd, and lidocaine ranked 57th. This could align with the narrow range of IC_{50} values, with a subtle trend observed where bupivacaine and ropivacaine perform better than lidocaine. It is important to note, however, that many designed compounds rank higher than these reference compounds **(Table S3)**.

Considering the IC_{50} values for $Na_V1.5$ in oocytes when utilizing a mixture of the *R* and *S* enantiomer, it becomes evident that bupivacaine possesses a lower IC_{50} value (4.51 μM [40]) when compared to lidocaine's IC_{50} (57.9 μM). This aligns with the ranking position for $Na_V1.5$ (as indicated in **Table S4**), where *R/S* bupivacaine are in 6 and 9 positions, while lidocaine occupied the 52nd position.

After analyzing the rankings separately, the ranking for each compound in each channel was compared, and the compounds with the most favorable positions, indicating the lowest total ranking values, were identified (Step 4, **Figure 2**). **Table 1** presents the ranking of the initial 25 compounds with the highest polypharmacological potential, while the complete ranking of all 65 studied compounds can be found in **Table S5**. The first 10 compounds (excluding the reference compounds) from the ranking were selected

for synthesis and subsequent electrophysiology experiments across the three channels.

Chemistry

The synthesis of the compounds was conducted through two consecutive steps:

1) Formation of the amide bond, and

2) Nucleophilic substitution.

For the amide bond formation, the coupling reagent DIC was utilized, recognized as one of the most extensively employed carbodiimide-type reagents [47]. Its use has demonstrated advantages in amide formation [47,48] in comparison to traditional methodologies [49,50].

In the initial phase, the amide was synthesized (as depicted in **Scheme 1**) using the DIC coupling reagent. This reaction spanned 1 hour and yielded between 96% and 98%. Following the acquisition of the amide product, it underwent purification and drying. Subsequently, the following phase of the reaction involved substituting the bromine of the amide with a secondary amine, culminating in the production of the final compound. This reaction extended over 24 hours and was monitored using TLC. Thereafter, the process encompassed ethyl acetate extraction, succeeded by washes with water, sodium bicarbonate solution, and sodium chloride solution. Ultimately, the compounds underwent purification through column chromatography, utilizing ethyl acetate: petroleum ether mixtures as the eluant. The compounds were obtained with yields ranging from moderate to good, spanning between 55% and 84%, and displayed high purity levels. The results are presented in **Figures 3, S1 – S57**.

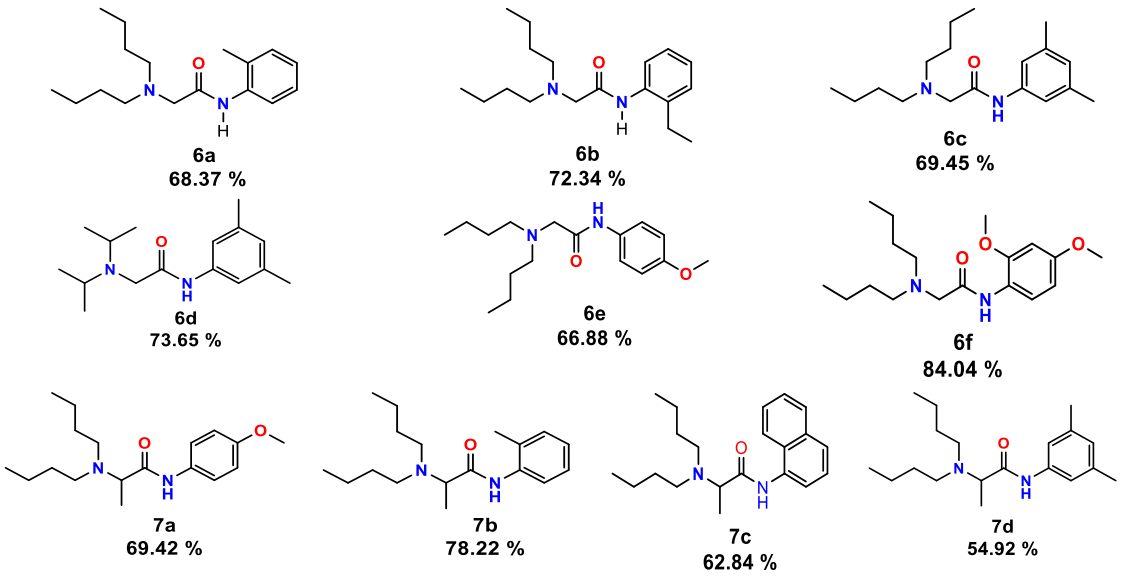

Figure 3. Structure of compounds **6a-6f** and **7a-7d** and their Yield.

Biological Assay

Preliminary testing

The two-electrode voltage clamp (TEVC) technique was employed to conduct electrophysiology tests. The initial step involved expressing each of the channels in a heterologous system of *Xenopus laevis* oocytes. For this purpose, the cells were injected with cRNA at a concentration of 50 ng/µL and maintained at a temperature of 16 °C for 24 to 48 hours until the channel expression occurred. To gain an initial understanding of the compounds' potential to block the channels, measurements were taken at a concentration of 100 µM for the 10 synthesized compounds on the TASK-1 and K_V1.5 channels.

To identify the most effective compounds capable of simultaneously inhibiting the TASK-1 and K_V1.5 channels, a comparison of the inhibition results for both channels was conducted **(see Figure 4)**. The recordings of the compounds in the K_V1.5 channel exhibit varying levels of inhibition, but significantly lower than in TASK-1 (p-value,

<2e-16. **Table S6**). While all the compounds exhibit some degree of blockade on this channel, it is notable that compounds **6f**, **6e**, **7a**, and **7b** show the highest activity, demonstrating blocking percentages of approximately 55.75 ± 5.16%, 42.22 ± 9.50%, 38.04 ± 7.20% and 36.86 ± 6.10%, respectively in K_V1.5. Conversely, compounds **7c**, **6a**, **6b**, **6c**, **7d**, and **6d** display lower blocking percentages: 35.68 ± 8.18%, 33.86 ± 3.85%, 33.53 ± 4.12%, 16.43 ± 5.98%, 18.16 ± 3.64%, and 12.31 ± 2.69%, respectively in K_V1.5. In the case of the TASK-1 channel, all compounds exhibit a blockade exceeding 77%. Particularly, compounds **7c**, **6a**, and **6f** show the highest percentages of inhibition, at 89.34 ± 3.28%, 88.32 ± 3.79%, and 84.09 ± 2.76 respectively. Upon comprehensive comparison of the results, it becomes evident that compounds **6e**, **6f**, **7a**, **7b**, and **7c** exhibit superior activities on both channels.

In terms of statistical significance, there are no differences in the block in TASK-1 for the ten different compounds (gray letters in Figure 4). Regarding K_V1.5, **6d** has no statistically significant differences compared to **6c** and **7d**, but it does with the other seven compounds because its blocking activity is the lowest (blue letters in Figure 4). When comparing the combined effect of each drug in both channels, **6d** exhibits statistically significant differences with **6f** block (p-value 0.0417, **Table S6**).

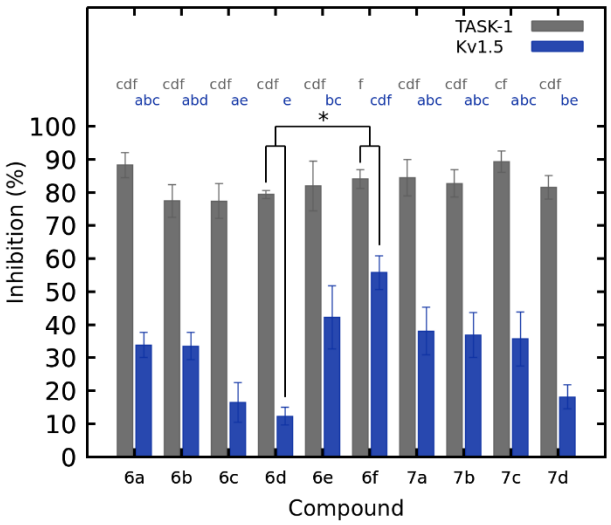

Figure 4. The inhibitory activity of compounds **6a-6f** and **7a-7d** were evaluated in TASK-1 and $K_V1.5$ channels using the TEVC technique at +40 mV and a concentration of 100 µM. For TASK-1; n=4 (**6e, 7a, 7b, 7c**), n=3 (**6a, 6b, 6c, 6d, 7d**), n=15 for **6f** and for $K_V1.5$; n=5 (except in **6a** and **7b**, where n =4). Data are presented as Mean ± SEM. Statistical significance is represented by letters indicating the individual effects of the compounds in each channel (gray letters for TASK-1 and blue letters for $K_V1.5$). There are no significant differences between drug blockades in a certain channel when they share the same letter. The combined effect, comparing compound blockades in both channels with another independent compound acting in both channels as well, is indicated with an asterisk.

The five compounds exhibiting the most pronounced activity on TASK-1 and $K_V1.5$ potassium channels were subjected to evaluation on $Na_V1.5$ **(Figure 5)**. At a concentration of 100 µM, compounds **6e**, **6f**, and **7b** demonstrated the highest efficacy on the channel, with inhibitions of 81.19 ± 4.25%, 62.39 ± 6.85%, and 58.91 ± 10.62%, respectively. Conversely, compounds **7c** and **7a** exhibited the lowest inhibitions at 31.10 ± 7.9% and 11.93 ± 4.16%, respectively, with the effect of compound **7a** approaching insignificance. Notably, compounds **6e** and **6f** share structural similarities, possessing an acetamide nucleus and butyl chains on the amine, differing in the number of methoxyl groups attached to the aromatic ring. Compound **6e** features one methoxyl group (in the 4-position), whereas compound **6f** displays two, located at carbons 2 and 4 of the benzene ring, respectively. As for compound **7b**, it retains aliphatic butyl chains

akin to the aforementioned compounds. However, its nucleus is propanamide, and the substituent on the aromatic ring is a methyl group at the 2-position. Compound **6f** emerges as the most effective in terms of simultaneous blocking activity across all three channels.

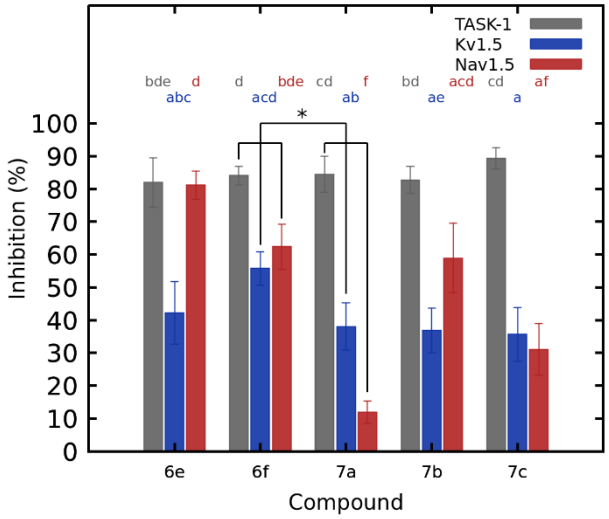

Figure 5. Inhibitory activity of compounds **6e, 6f, 7a, 7b** and **7c** were evaluated in the TASK-1 and $K_V1.5$ channels as mentioned in **figure 4** and in $Na_V1.5$ channels at -30 mV, at a concentration of 100 µM. For $Na_V1.5$; **6e** n=20, **6f** n=9, **7a** n=3, **7b** n=4, **7c** n=3. Data are presented as Mean ± SEM. Statistical significance is represented by letters indicating the individual effects of the compounds in each channel (gray letters for TASK-1 and blue letters for $K_V1.5$). There are no significant differences between drug blockades in a certain channel when they share the same letter. The combined effect, comparing compound blockades in both channels with another independent compound acting in both channels as well, is indicated with an asterisk.

In terms of statistical significance, compounds in $Na_V1.5$ channel exhibit varying levels of inhibition, but not very different from TASK-1 inhibition (p-value, 0.00845. **Table S6**) as with $K_V1.5$ inhibition (p-value < 0.001. **Table S6**). Analyzing the block in $Na_V1.5$ for the five different compounds (red letters in Figure 5), **7a** has no statistically significant differences compared to **7c**, but it does with the other three compounds because its blocking activity is the lowest. When comparing the combined effect of each drug in the three channels ($Na_V1.5$, $K_V1.5$ and TASK-1), **7a** exhibits

statistically significant differences with **6f** block (p-value 0.01115, **Table S6**).

IC_{50} determination

To determine the IC_{50} values for compound **6f** across each channel, dilution series were prepared. For $K_V1.5$, the concentrations used were: 1.0 µM, 10 µM, 35 µM, 100 µM, 350 µM, and 1000 µM. Similarly, for TASK-1 and $Na_V1.5$, the concentrations were: 0.01 µM, 0.1 µM, 1.0 µM, 10 µM, 100 µM, and 1000 µM. (Experiments were repeated a minimum of 3 times, with n=6.) **Figure 6** illustrates the IC_{50} curves for all three channels, with the values expressed in µM.

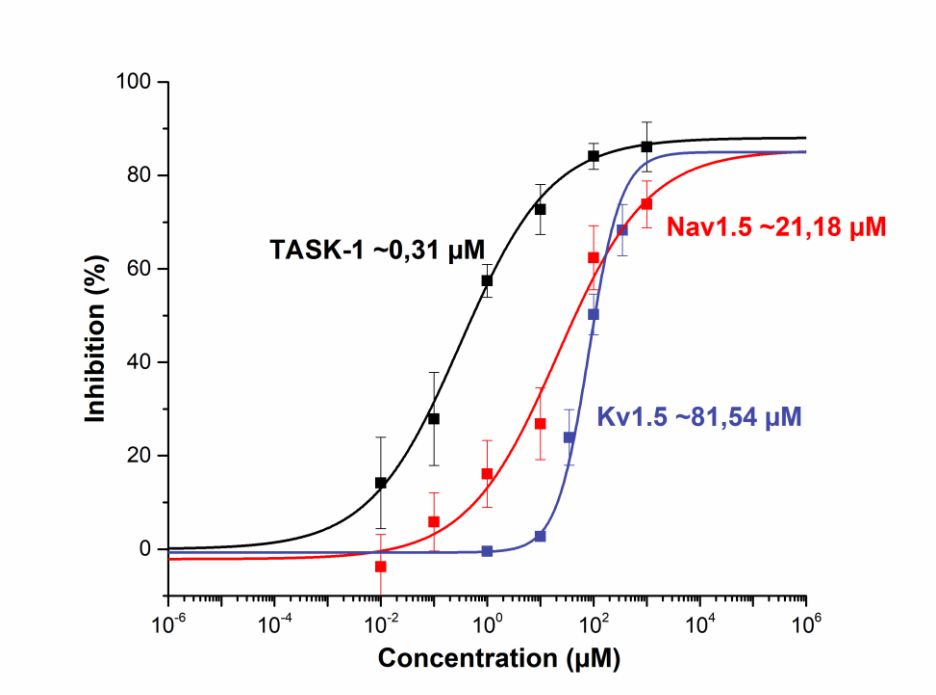

Figure 6. Inhibition curves (IC_{50}) for compound **6f** on TASK-1 and $K_V1.5$ channels. Block was analyzed at +40 mV. For $Na_V1.5$, the block was determined at -30 mV. For TASK-1 and $Na_V1.5$ the concentration range was from 0.01 µM to 1000 µM, and for $K_V1.5$ it was from 1 µM to 1000 µM. n= 6 -15.

Table 2 presents a comparison of the IC_{50} values with the reported data for LA, namely lidocaine, bupivacaine, and ropivacaine. Compound **6f** exhibits superior activity in the TASK-1 channel when compared to the mentioned LA. Regarding the

$K_V1.5$ channel, the IC_{50} value of compound **6f** is lower than that of ropivacaine and higher than that of bupivacaine. A comparison of **6f**'s activity with lidocaine is not possible due to the absence of reported activity on this channel. Finally, the activity of **6f** within the $Na_V1.5$ channel surpasses that of both lidocaine and ropivacaine. The IC_{50} used as reference for the LA in TASK-1 and ropivacaine in Nav1.5, were calculated in HEK-293 cells. While the IC_{50} reported here were measured in *Xenopus laevis* oocytes. Considering the previously reported magnitude differences in IC_{50} when both systems are compared [39,51], it is possible that the IC_{50} values reported here would be much lower if evaluated in HEK-293 cells.

Table 2. Reported IC_{50} values for LA vs Compound **6f**.

Ionic Channel	Lidocaine	Ropivacaine	Bupivacaine	Compound 6f
TASK-1	53.8 µM[a] [39]	17.6 µM[a,c] [39]	12.1 µM[a,c] [39]	0.31 µM[b]
$K_V1.5$	NR	128.9 µM[b,d] [16]	31 µM[b,c] [16]	81.5 µM[b]
$Na_V1.5$	57.9 µM[b,e]	322.2 µM[a,c,f] [41]	4.5 µM[b,c] [40]	21.2 µM[b]

a. Measurements in HEK-293 cells.
b. Measurements in *X. laevis* oocytes
c. *R/S*
d. *S*
e. Data provided by the Laboratory of Philipps-University Marburg, Germany.
f. IC_{50} measured in $Na_V1.5$ open state, as was measured using our pulse protocol.
NR: Not reported.

These results are consistent and validate the proposed design of the polypharmacological ranking. The top-performing compound, **6f**, exhibited the highest activity across all three channels and is positioned second within the compound ranking **(Table 1)**. In terms of individual channel rankings, in the $K_V1.5$ channel, compound **6f** occupied the 4th position in the CC dockings **(Table S1)** and the 10th position in the side-pocket dockings **(Table S2)**.

Similarly, other compounds closely resembling the activity of **6f** in $K_V1.5$—namely **6e**, **7b**, and **7c (Figure 5)** achieved rankings greater than 10 in the CC dockings but occupied positions 2, 3, and 6 respectively in the side-pocket dockings. Compound **7a** emerged as the leading candidate in the CC dockings and held the 9th position in Kv1.5 SP dockings **(Tables S1-S2)**.

Regarding TASK-1, compound **6f** occupies the 10th position in the docking ranking **(Table S3)**. Leading this ranking are compounds such as **7a**, **7b**, **6a**, **6c**, and **6d**, which exhibit similar blocking percentages in the TASK-1 channel **(Table S3)**.

Turning to the $Na_V1.5$ channel, compound **6f** holds the first position in the ranking **(Table S4)**, while **6e**, with a similar—perhaps even higher—blocking percentage in the $Na_V1.5$ channel **(Figure 5)**, is also among the top 10 compounds in the ranking.

Selectivity

Once the simultaneous blockade of compound **6f** on the TASK-1, $K_V1.5$, and $Na_V1.5$ channels was established, other cardiac channels including $K_{ir}2.1$, TREK-1, and TASK-4 were selected to assess the compound's selectivity. Measurements were conducted at a concentration of 100 µM **(Figure 7)**.

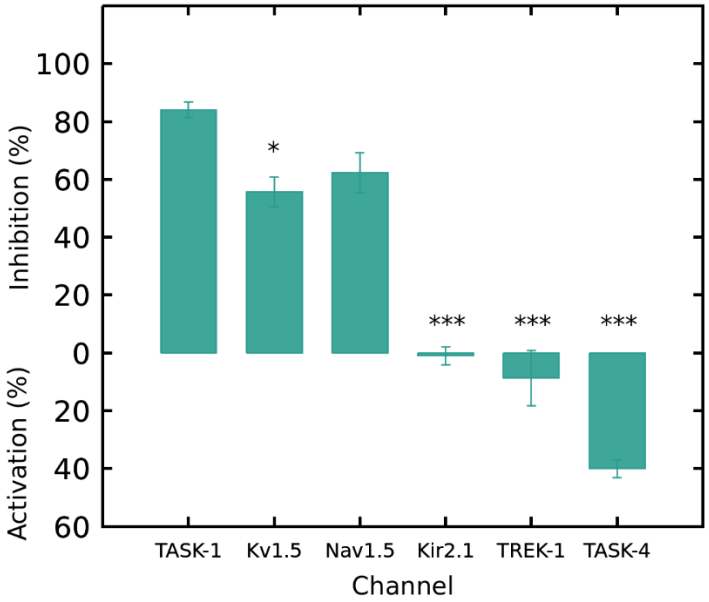

Figure 7. The activity of compound **6f** on different channels was analyzed at100 µM by TEVC in *X. laevis* oocytes. All data is presented as mean ± SEM. The experiments were replicated as follows; TASK-1 n=4, $K_V1.5$ n=5, $Na_V1.5$ n=9, $K_{ir}2.1$ n=3, TREK-1 n=4 and TASK-4 n=3.

$K_{ir}2.1$ channel is found in various cell types, including cardiac myocytes [52] . It is considered essential for generating repolarization current in ventricular AP and is downregulated in patients with cardiac failure [53], but upregulated in AF [54]. The compound had no significant effect on this channel (-1.01% ± 3.05%).

Another channel related to ventricular repolarization, the TREK-1 channel, was also evaluated. While its role in the heart is still controversial [55], it is expressed in both the atria and ventricles [56,57], with greater expression in the ventricles [58]. Inhibition of TREK-1 has been suggested to have arrhythmogenic effects in the ventricles [55,59]. Some antiarrhythmic drugs like dronedarone [60], ranolazine [61], lidocaine [62], and carvedilol [63], among others [64], have been reported to block TREK-1 currents. However, the contribution of this inhibition to their clinical antiarrhythmic effects has not been conclusively established [55]. Moreover, downregulation of TREK-1 was established in a model of AF due to cardiac remodeling

[58,65]. In this context, it is relevant to evaluate the effect of **6f** on the TREK-1 channel. The compound did not inhibit the channel; instead, it showed a non-significant activating effect (-8.71% ± 9.61%).

Finally, the TASK-4 channel, another cardiac channel within the K_{2P} family and a recognized pharmacological target for atrial and ventricular arrhythmias [66], was evaluated. TASK-4 is primarily expressed in the atria [19], and its expression is reduced in patients with heart failure and AF [20]. Consequently, it has been proposed that channel activation could represent an antiarrhythmic strategy [66].

In the case of compound **6f** at the concentration evaluated (100 µM), a moderate activation of the TASK-4 channels (40.0% ± 3.2%, n=3) was observed, similar to what has been reported in previous studies with antiarrhythmics [66] such as vernakalant, an antiarrhythmic for clinical use in AF [67]. To summarize, the predominant effect of **6f** blockade on the TASK-1, $K_V1.5$, and $Na_V1.5$ channels indicates a higher affinity for these channels compared to what was observed for the other evaluated cardiac channels. Notably, with the exception of the K_2P channel TASK-4, where **6f** showed activation.

Patch-clamp recordings on isolated human atrial cardiomyocytes

Compound **6f**, the most effective blocker of the TASK-1, $K_V1.5$ and $Na_V1.5$ channels in *X. laevis* oocytes, was further evaluated in patch-clamp experiments on single atrial cardiomyocytes isolated from tissue samples of patients undergoing cardiac surgery for Coronary Artery Bypass Grafting (CABG), Aortic Valve Replacement (AVR) or heart transplantation **(Table S7).**

In cardiomyocytes obtained from patients with sinus rhythm (SR), we observed a concentration-dependent decrease in the action potential amplitude (APA) and in the maximal upstroke velocity (dV/dt_{max}) compared to baseline that reached statistical significance at a concentration of 12.5 µM ($p < 0.05$) **(Figure 8A, 8B and 8C)**, which is consistent with the $Na_V1.5$ block that we have observed by **6f** in TEVC recordings **(Figure 6,** [68]**)**. In contrast, only minor effects on the APD_{50} and APD_{90} were recorded **(Figure 8D, 8E**), with no clear trend towards a concentration-dependent increase or decrease. No statistically significant effects on the resting membrane potential were observed **(Figure 8F).**

In cells obtained from tissue samples of AF patients, we did not observed changes in APA and in the maximal upstroke velocity compared to baseline (**Figure 8G, 8H, 9I)**. However, we noted a differential effect on the APD compared with cells isolated from SR patients. Previous studies have shown that the expression of the TASK-1 channel is upregulated in atrial cardiomyocytes in AF-patients, causing an AP shortening [19,20]. Consistent with the results of our voltage-clamp experiments indicating a high affinity of compound **6f** for this channel, both APD_{50} and APD_{90} showed a clear trend towards a concentration-dependent prolongation in the AF cohort **(Figure 8J and 8K)**, although the effect sizes did not reach statistical significance at concentrations of 1 µM and 12.5 µM. The increase in ADP_{50} with 6.25 µM **6f** in AF cells was significantly different from baseline. Interestingly, we also recorded a significant concentration-dependent shift of the resting membrane potential to more negative values in this cohort **(Figure 8L),** which might be based on the TASK-4 activation by **6f (Figure 7)**.

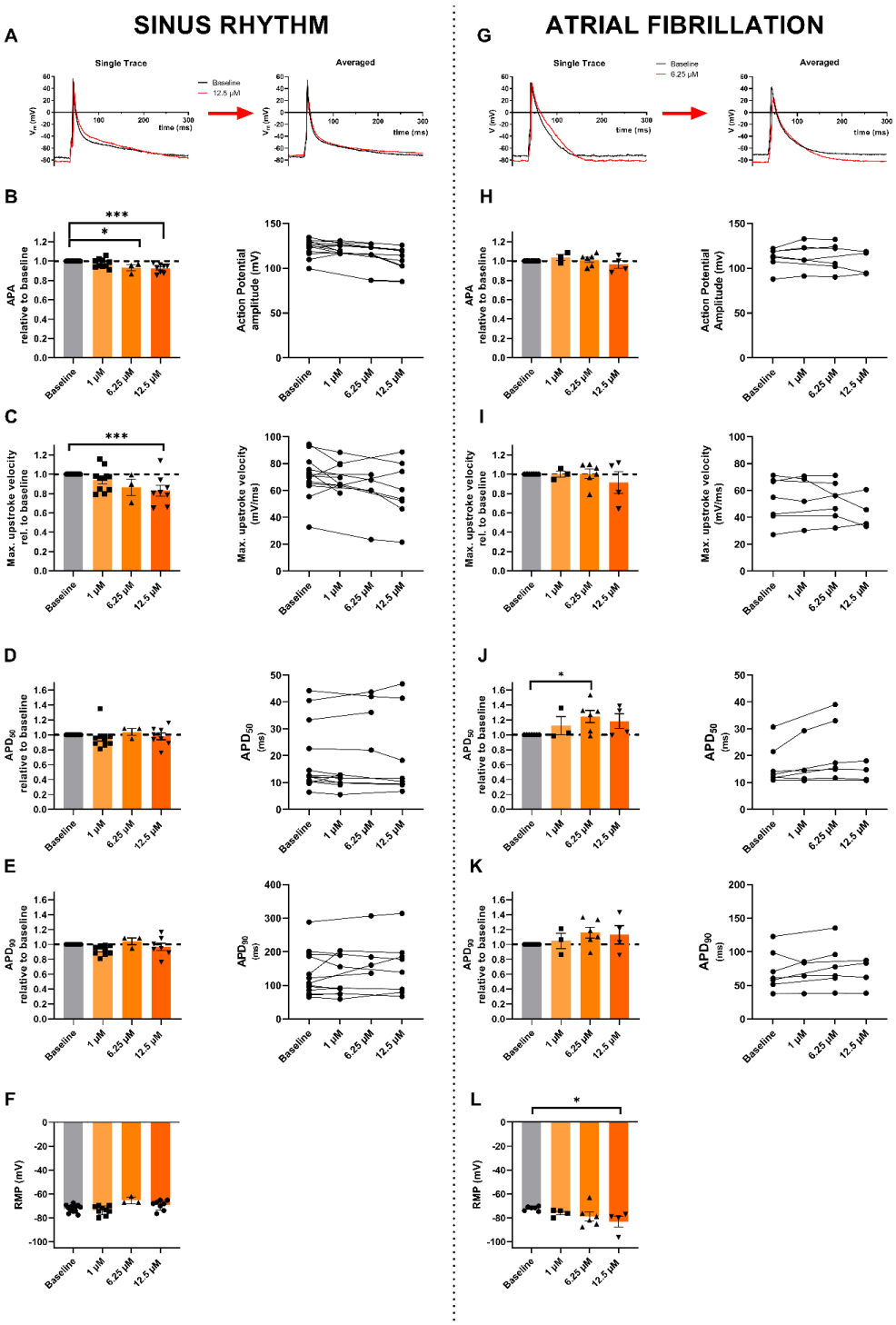

Figure 8. Comparative analysis of patch-clamp recordings of single atrial cardiomyocytes isolated from tissue samples of patients in sinus rhythm (A – F; n=13/N=5) and with atrial fibrillation (G – L; n=6/N=5). A and G) *Left:* Representative single AP traces from patch-clamp recordings under basal conditions (Baseline, black) and 8 – 10 mins after application of compound 6f. *Right:* AP traces averaged over 4 distinct recordings under baseline conditions (black) and 8 – 10 mins after application of compound 6f. B and H) *Left:* Recorded changes in AP-amplitude relative to baseline (%) after application of compound 6f. *Right:* Absolute values for the AP-Amplitude (mV) at baseline and after application of compound 6f at concentrations of 1 µM, 6.25 µM, 12.5 µM for individual recordings. C and I) *Left:* Recorded changes in the maximum upstroke velocity relative to baseline (%)

after application of compound 6f. *Right:* Absolute values for the maximum upstroke velocity (dv/dt_{max}) at baseline and after application of compound 6f for individual recordings. D and J) *Left:* Recorded changes in the APD_{50} relative to baseline (%) after application of compound 6f. *Right:* Absolute values for the APD_{50} (ms) at baseline and after application of compound 6f for individual recordings. E and K) *Left:* Recorded changes in the APD_{90} relative to baseline (%) after application of compound 6f. *Right:* Absolute values for the APD_{90} (ms) at baseline and after application of compound 6f for individual recordings. F and L) Recorded resting membrane potentials (mV) at baseline and after application of compound 6f at the abovementioned concentrations. Data are given as mean ± standard error of the mean. Individual columns were compared to baseline using one-way ANOVA with Dunnett's post-hoc-test. *indicates a p-value of <0.05; *** indicates a p-value of <0.001.

The effects of the **6f** compound in single atrial cardiomyocytes partially resemble those of vernakalant, an atrial-selective antiarrhythmic drug that reduces APA by blocking Na^+ channels [69]. Additionally, vernakalant activates TASK-4 channels [67] and it is a blocker of $K_V1.5$ channels [70]. However, vernakalant does not significantly reduce TASK-1 currents [71]. The overall effect of vernakalant on action potential duration is small in human right atrial tissue [69].

These similarities and differences could be understood based on the chemical structural features shared by **6f** and vernakalant (**Figure 9**). Both exhibit a common pharmacophore with hydrophobic, hydrogen acceptor groups, and an aromatic ring. These features are also shared by the local anesthetics bupivacaine, ropivacaine, and lidocaine. However, vernakalant differs in the hydrogen donor group (the NH atoms of the amide linker), which is not present in its structure but is present in both local anesthetics and 6f compounds (**Figure 1**).

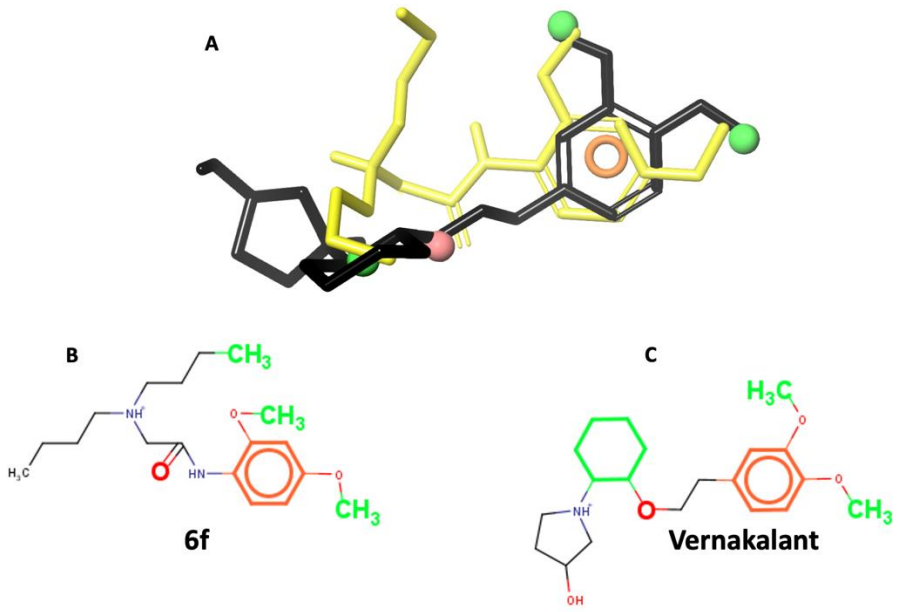

Figure 9. Common pharmacophore to 6f and vernakalant. A) Compounds **6f** (yellow) and vernakalant (black) are shown in sticks representation. Green and red spheres stand for hydrophobic and hydrogen acceptor groups, respectively. Orange halo represents an aromatic ring. B and C) Pharmacophoric features represented in **6f** and vernakalant, respectively, using the same colors as in A. Notice that the NH atoms of the amide linker (-CONH-) are not present in vernakalant.

***In-silico* Trials for the Pharmacological Management of AF by Compound 6f**

The efficacy of compound **6f** for both acute AF cardioversion and long-term AF prevention was subsequently assessed in a digital twin population of 45 virtual human atria. **Figure 10** illustrates the impact of three concentrations (1, 10, and 100 μM) of compound **6f** on the APD (panels A and B), effective refractory period (panel C), efficacy of acute cardioversion, efficacy of long-term AF prevention (panel D), and AF duration (panel E).

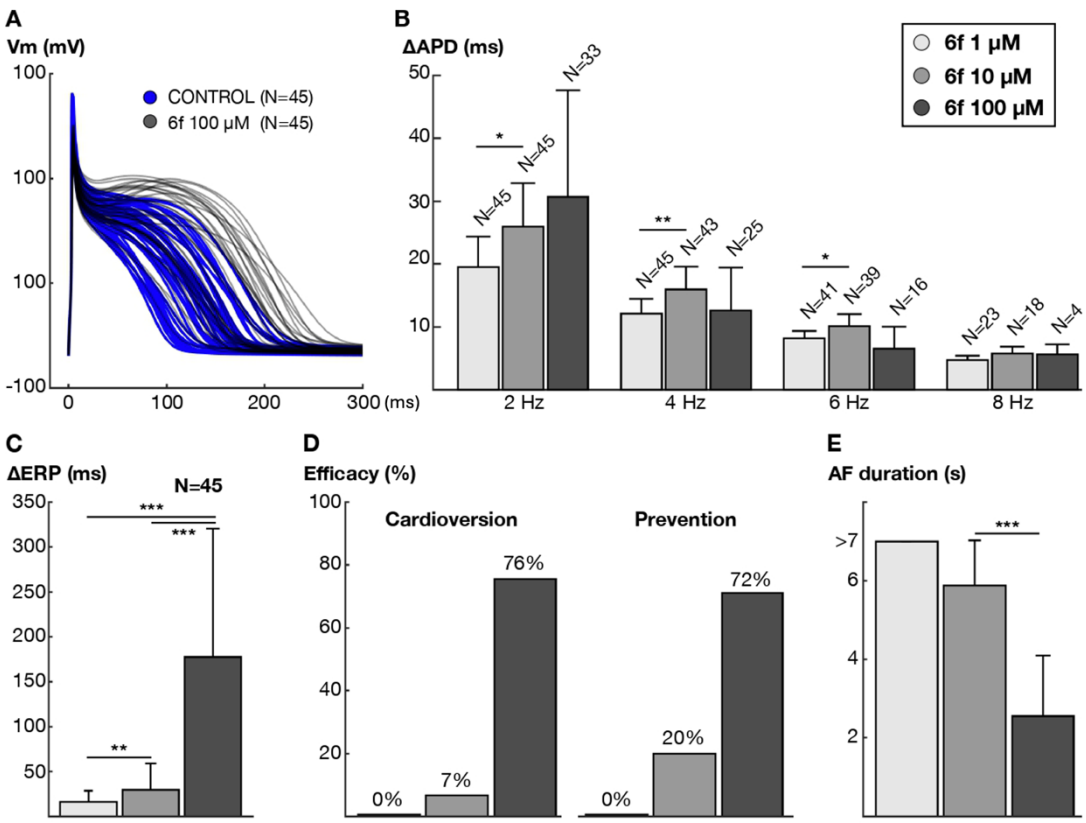

Figure 10. Impact of three concentrations (1, 10 and 100 µM) of compound **6f** on single cell and whole-atria properties. A) AP traces of N=45 atrial cardiomyocyte models at 2Hz in control conditions and after the application of compound **6f** at 100 µM. B) Rate-dependent variation of the APD (ΔAPD). "N" indicates the number of atrial cardiomyocyte models able to propagate the stimulus according to the concentration applied and the pacing rate. C) Concentrations-dependent increase in the effective refractory period (ΔERP) compared to control conditions in the N=45 atrial cardiomyocyte models. D) AF cardioversion and prevention efficacy (i.e., percentage of AF episodes cardioverted or prevented) in the population of 45 virtual-atria models. E) AF duration in the 45 virtual-atria models considering that AF episodes are analyzed for 7 s of activity.

Consistent with the experimental results in cardiomyocytes from AF patients, the application of compound **6f** resulted in the prolongation of the APD at the cellular level (142.2±30.7 vs. 181.6±38.8 for control vs. compound **6f** at 100 µM at 2 Hz; N=45; **Figure 10A**). Subsequently, the *in-silico* atrial cardiomyocytes were paced on a one-dimensional cable to assess propagation properties and refractoriness. At moderate frequencies (i.e., 2 Hz), the virtual administration of compound **6f** induced a concentration-dependent prolongation of the APD. With an increase in pacing frequency,

less cardiomyocyte models were capable of propagating the stimulus after applying compound **6f** at 100 μM, due to longer post-repolarization refractoriness (87% [39/45] vs. 35% [15/45]) of cardiomyocyte models propagating the stimulus at 6 Hz after 10 μM vs. 100 μM of compound **6f**; **Figure 10B**). At these higher rates, the pronounced inhibition of sodium current (I_{Na}) prevailed over the blockade of potassium currents (I_{Kur} and I_{K2P}), resulting in a greater APD prolongation with 10 μM than with 100 μM (**Figure 10B**; from 4 Hz to 6 Hz).

The concentration-dependent prolongation of post-repolarization refractoriness is depicted in **Figure 10C**. Application of 1 μM, 10 μM, and 100 μM of compound **6f** increased the refractory period by 16.3±12.3 ms, 29.3±29.5 ms, and 177.6±143.0 ms, respectively, compared to control conditions. This elevation in refractoriness led to a proportional enhancement in the effectiveness of compound **6f** for rhythm control of AF **(Figure 10C and 10D)**. Consequently, its virtual administration to a population of 45 whole-atria models resulted in a concentration-dependent increase in AF cardioversion and prevention efficacy **(Figure 10D)**. This effect was also evident in the overall reduction in AF duration following application of compound **6f** at 100 μM (**Figure 10**). **Figure 11** presents a representative AF episode under control conditions and after the virtual administration of 10 and 100 μM of compound **6f**, illustrating the reduction of AF burden with increasing concentrations. The drug was administered 2 s after AF initiation, representing acute AF cardioversion.

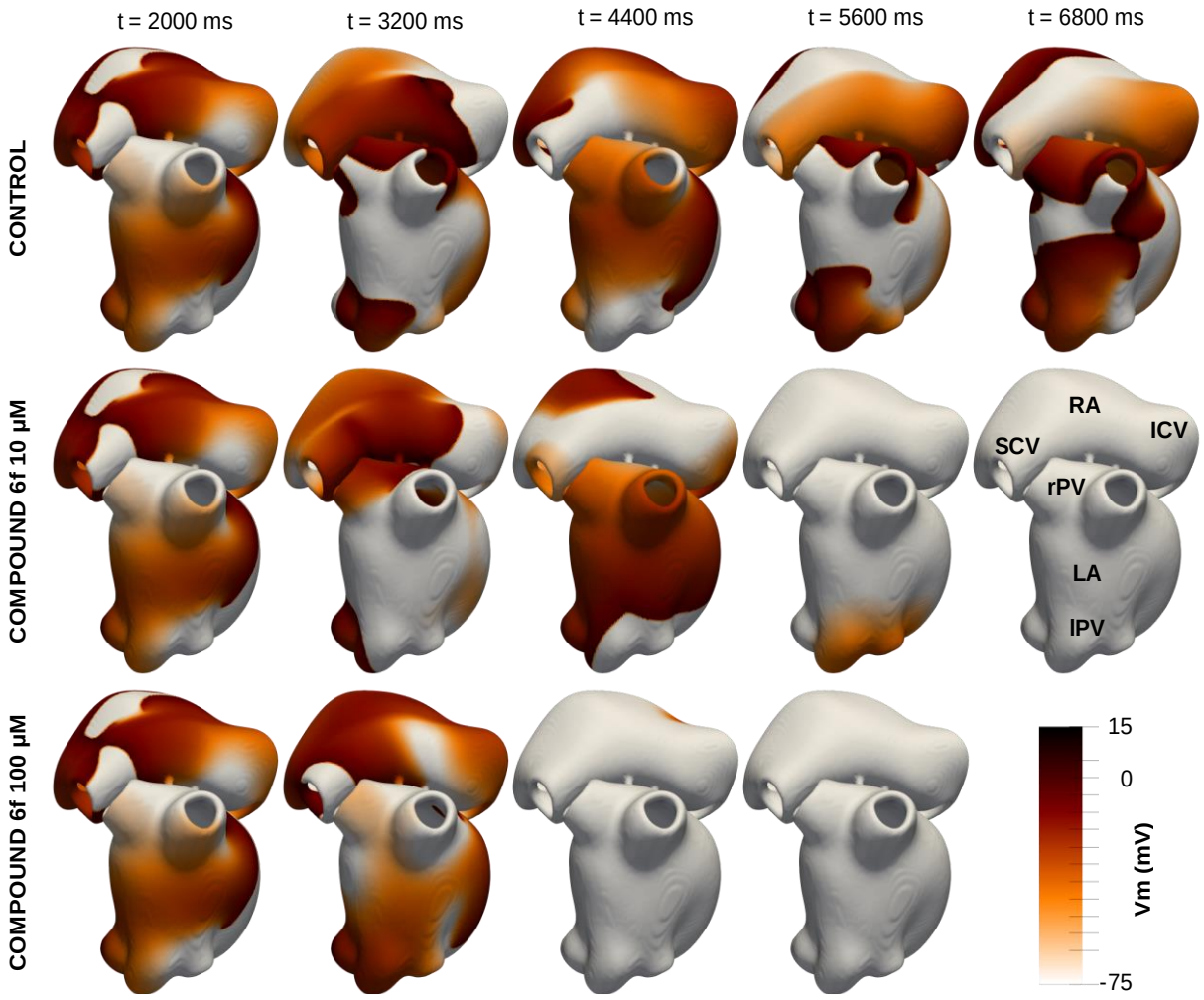

Figure 8. Consecutives snapshots of the transmembrane voltage (V_m) for a representative AF episode in control conditions and after the virtual administration of 10 and 100 µM of compound **6f**. Abbreviations: RA-LA: Right and left atrium; SCV-IVC: Superior and inferior cava vein; rPV-lPV: Right and left pulmonary veins

Predictions of pharmacokinetics

To assess the potential strengths and weaknesses of the synthesized compounds for their suitability as drugs, their properties were analyzed from both a physicochemical and pharmacokinetic perspective using the SwissADME platform [72]. The results are presented in **Table 3**, together with LA properties for comparative purposes. These analyses offer a theoretical prediction of the molecules' viability according to Lipinski's rule of five [73] and pharmacokinetic parameters.

Table 3. Pharmacokinetic parameters of the evaluated compounds vs LA.

Compound	Physicochemicals				Pharmacokinetics						Lipinski rule violations
	DH[a]	AH[b]	LogPo/w[c]	GIA[d]	P-gp[e]	CYP1A2[f]	CYP2C19[f]	CYP2C9[f]	CYP2D6[f]	CYP3A4[f]	
6a	1	2	3.53	High	No	Yes	No	No	Yes	Yes	0
6b	1	2	3.81	High	No	Yes	No	No	Yes	Yes	0
6c	1	2	3.92	High	No	Yes	No	No	Yes	No	0
6d	1	2	3.15	High	No	No	No	No	Yes	No	0
6e	1	3	3.24	High	No	Yes	No	No	Yes	No	0
6f	1	4	3.36	High	No	Yes	No	No	Yes	No	0
7a	1	3	3.62	High	Yes	Yes	No	No	Yes	No	0
7b	1	2	3.92	High	Yes	Yes	No	No	Yes	No	0
7c	1	2	4.54	High	Yes	Yes	Yes	Yes	Yes	Yes	0
7d	1	2	4.30	High	Yes	No	No	No	Yes	Yes	0
lidocaine	1	2	2.50	High	No	No	No	No	Yes	No	0
ropivacaine	1	2	3.05	High	No	No	No	No	Yes	No	0
bupivacaine	1	2	3.40	High	No	No	No	No	Yes	No	0

a. DH: N° hydrogen donor bonds (≤ 5)
b. AH: N° hydrogen acceptor bonds (≤ 10)
c. Log Po/W: Octanol/water partition coefficient (≤ 5)
d. GIA: Gastrointestinal Absorption
e. P-gp: Permeability glycoprotein substrate. If Yes, it is substrate for P-gp.
f. CYP: Isoenzymes belonging to the cytochrome P450. If No, it is not an inhibitor of a given CYP.

None of the synthesized compounds or the LA violate any Lipinski's rule: poor absorption or permeation with more than 5 hydrogen bond donors, presence of 10 hydrogen acceptors, molecular weight exceeding 500 Da, and octanol/water partition coefficient surpassing 5 [73]. All the compounds examined displayed the potential for gastrointestinal absorption (GIA). This suggests that they have the capacity to be promising candidates for oral drug development.

We also assess the behavior of the compounds as substrates for the permeability glycoprotein (P-gp), which holds significant importance for facilitating the efflux of xenobiotics across biological membranes in the gastrointestinal tract or the brain [74]. Furthermore, the compounds' role in relation to the isoenzymes within the cytochrome P450 (CYP) family was established. This information enables us to determine the likelihood of these molecules to interact through CYP inhibition and identifies which specific isoforms are affected [72], because being a substrate for P-gp and/or not

inhibiting CYP isoforms is key in biotransformation and elimination of the drug [75]. In this context, all the compounds exhibit characteristics of being P-gp substrates and/or can undergo processing by CYPs. This information holds significant relevance, as CYP and P-gp can collaboratively process small molecules, contributing to tissue protection—a vital aspect concerning drug bioavailability and toxicity.

This analysis suggests that the synthesized compounds could potentially evolve into effective drugs with favorable bioavailability and minimal toxicity.

Cytotoxicity assay: hemolysis

Relying solely on assays in cardiomyocytes and Xenopus oocytes is not always sufficient to determine the safety of a compound, as these assays do not cover all possible effects on different cell types and tissues. Furthermore, it is essential to perform a variety of *in vitro* and *in vivo* assays to fully understand the potential effects of the compound on different biological systems and thus determine its safety and efficacy in clinical contexts.

A recommended method to evaluate cytotoxicity in molecules with biological activity is hemolysis, which consists of evaluating the rupture of erythrocytes and, consequently, the release of hemoglobin. Since free hemoglobin in the plasma can potentially cause damage to various vital organs, this poses a risk of toxicity and affects the routes of drug administration, including intravenous and other methods [76]. Therefore, hemoglobin release was used to quantify whether the most active compounds in $K_V1.5$ and TASK-1, selected for further analysis in $Na_V1.5$ (**Figure 5**), might tend to disrupt membranes.

Erythrocytes treated with tween-20 and phosphate buffer were used as 100% and 0% hemolysis value, respectively. Red blood cells (RBCs) were incubated with different concentrations of compounds **6e, 6f, 7a, 7b,** and **7c** ranging from 0.2 to 400 μM for two hours. The compounds tested did not show a hemolytic effect at the concentrations tested, suggesting that they do not detectably affect the red blood cell membrane. The results of the assays using the highest concentration (400 μM) are presented in **Figure 12**.

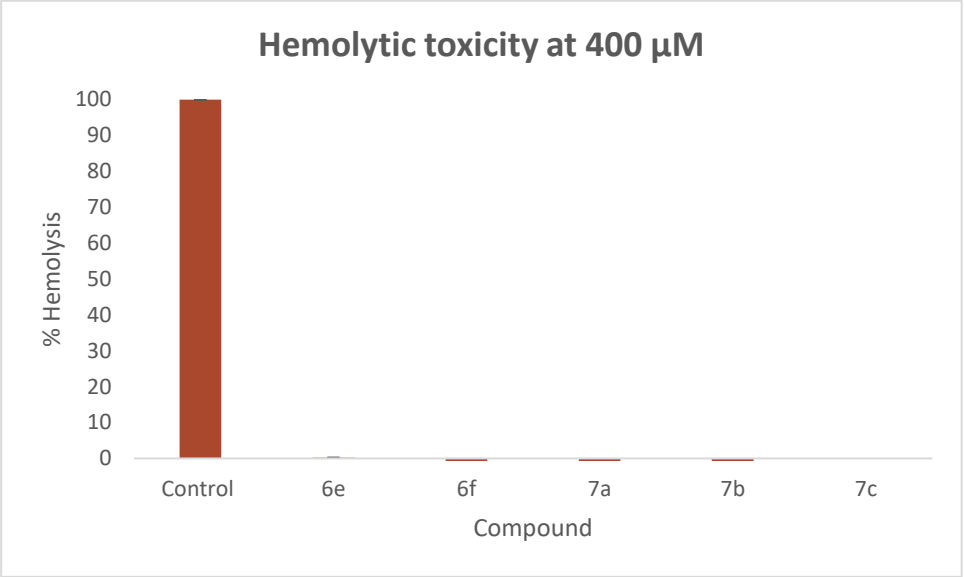

Figure 12. Hemolytic activity of compounds **6e**, **6f**, **7a**, **7b** and **7c** at 400 µM in human erythrocytes measured at 504 nm. All data are presented as mean ± SEM. The experiments were in triplicate n=3.

Conclusions

In this study, a series of 60 molecules was designed rationally based on the pharmacophore for LA, compounds known for their use as antiarrhythmics and their simultaneous blockade of the $Na_V1.5$, $K_V1.5$, and TASK-1 channels. Following the proposal of these candidate molecules, molecular docking calculations were conducted, assuming that the designed compounds could possess binding sites similar to those reported for LA. The BS of LA are determined for bupivacaine in TASK-1 [44], bupivacaine and ropivacaine in $K_V1.5$ [16], and lidocaine in $Na_V1.5$ [43,77,78]. Subsequently, employing the results of molecular docking and MM-GBSA calculations, a ranking was formulated to identify the most promising candidates. Notably, several designed compounds exhibited *in-silico* outcomes superior to those of reference compounds.

Having identified the optimal compounds, synthetic pathways were optimized through assessment of various strategies. The chosen compounds, namely **6a-f** and **7a-d**, were synthesized in two steps: an acylation employing the coupling reagent DIC, followed by a

substitution phase. These synthesized compounds were subsequently purified and characterized, yielding moderate to good yields.

Initial biological tests involving the application of compounds at 100 µM on the potassium channels TASK-1 and $K_V1.5$ through the two-electrode voltage-clamp method demonstrated robust current inhibition, particularly evident in the TASK-1 channel. Among the compounds tested, namely **6e**, **6f**, **7a**, **7b**, and **7c**, the best inhibitory capacities across both systems (TASK-1 and $K_V1.5$) were observed. Furthermore, evaluation on the $Na_V1.5$ channel indicated that compounds **6e**, **6f**, and **7b** exhibited the most substantial blocking percentages.

Compound **6f** exhibited the most potent blocking activity across all three channels, specifically TASK-1, $K_V1.5$, and $Na_V1.5$, at the micromolar level, with values of 0.31, 81.5, and 21.18, respectively. The IC_{50} values of compound **6f** indicate its capability to concurrently inhibit TASK-1, $K_V1.5$, and $Na_V1.5$ channels, often demonstrating greater affinity compared to LA. This trend highlights its potential as a multi-target agent. Evaluations on other cardiac channels such as $K_{ir}2.1$ and TREK-1, revealed either negligible or minimal activity of the compound relative to its effect on the target channels. However, in the K_2P channel TASK-4, **6f** exhibited approximately 40% activation at 100 µM.

In patch-clamp recordings on isolated human atrial cardiomyocytes, we detected a concentration-dependent decrease in APA and in the maximal upstroke velocity in patients with SR, which is consistent with the $Na_V1.5$ block that we have observed by **6f**. In cells obtained from tissue samples of AF patients, we noted a significant increase in

ADP_{50} when applying 6.25 µM of **6f**. This finding aligns with the results of voltage-clamp experiments, demonstrating a high affinity of compound **6f** for the TASK-1 channel. Additionally, in this cohort, we observed a significant concentration-dependent reduction in the RMP towards more negative values, consistent with TASK-4 activation by **6f**.

Simulations of whole-atria showed potentially favorable effects of compound **6f** in atrial fibrillation (AF). It prolonged the action potential duration (APD) and refractory period in a concentration-dependent manner. Furthermore, **6f** exhibited the capacity to induce cardioversion, suggesting its potential as a prospective drug for both managing and preventing AF.

Diverse physicochemical and pharmacokinetic parameters were evaluated for the ten synthesized compounds. The findings demonstrated that, akin to LA, they do not violate any of Lipinski's rules. Compound **6f** complies with the Lipinski rules and shows the potential to be metabolized by at least two CYP enzymes.

Finally, a hemolysis assay showed that the most active compounds in $K_V1.5$ and TASK-1, selected for further analysis in $Na_V1.5$, do not disrupt membranes. All this evidence potentially elevates the synthesized compounds and particularly **6f** as candidates drugs for AF.

Experimental procedures

Computational studies

In summary, we conducted a protocol to identify drugs with the highest polypharmacological potential by performing Induced Fit Docking (IFD) of 60 compounds

in TASK-1, $Na_V1.5$, and $K_V1.5$ channels. To perform IFD, the grid was centered at the fenestrations in TASK-1, the CC of $Na_V1.5$, and the CC and SP of $K_V1.5$. Subsequently, the binding free energy of each pose generated by IFD was calculated for each ligand-channel complex. A ranking of the compounds was then proposed to select the top 10 compounds for synthesis and subsequent electrophysiology experiments.

Computational Studies: Design and Selection of the compounds

Based on the LA pharmacophore [77,79–81], we designed two series of 60 compounds as follows: 30 compounds derived from bromoacetic acid **(Figure 2A)** and 30 compounds derived from (*S*)-2-bromo-propionic acid **(Figure 2B)**. IFD calculations of the 60 proposed candidates were carried out in the three different channels (TASK-1, $K_V1.5$, and $Na_V1.5$). Before the molecular docking step, the ligands were drawn using the Maestro workspace and then refined using "LigPrep" (LigPrep, Schrödinger, LLC, New York, NY, 2023). The "Epik" [82] module included in Maestro Schrödinger 11.8 suite was employed to establish the protonation form of the amino group. Finally the ligands were energetically minimized using the conjugate gradient method [83] implemented in the Macromodel module until energy convergence was achieved.

In parallel, we prepared the protein structures to avoid steric hindrances. For TASK-1, we utilized the TASK-1 crystal structures (PDB: 6RV3, chains A, B) [84], and for $Na_V1.5$, we used the $Na_V1.5$ crystal structures (PDB: 6LQA) [85]. As for the $K_V1.5$ channel, we employed the homology model proposed by Marzian et al., 2013, which was based on the crystal structures of the open-state chimera $K_V1.2$: $K_V2.1$ (K_VChim) (PDB template: 2R9R) [17]. This homology model has been successfully used in several research studies

[16,26,86]. The structures were prepared using the "Protein Preparation Wizard" [87] module of the Schrödinger suite software. Charges and parameters were assigned according to the OPLS-2005 force field. The missing residues in TASK-1 (149-151 from chain A and 150-151 from chain B) were modeled using the "crosslink protein" tool from the Schrödinger suite. For TASK-1, additional molecules present in the structure were removed prior to preparation, retaining only the protein and ions in the selectivity filter. In the $K_V1.5$ model, 2 ions and 2 water molecules present in the selectivity filter were retained, and the $Na_V1.5$ structure was used without any additional molecules. The protonation states of the structures were predicted at a pH of 7.0 using PROPKA [88].

To perform the molecular docking, the Induced Fit Docking (IFD) protocol was used, which utilizes the Glide software incorporated in the 11.8 Schrödinger suite [45] and the standard precision (SP) scoring function, yielding a maximum of 10 poses *per* docking calculation. The grid centers for all systems were defined internally in the IFD protocol as the geometric center of each binding site of the LA and their values are updated according to the movement of the side chains in the different docking refinement steps of the protocol. For TASK-1, a single lateral fenestration was explored, as both subunits are symmetrical. Fenestration exploration was based on binding site (BS) residues **(Table 4)** reported for bupivacaine [44]. In the case of $K_V1.5$, the residues reported as crucial for the binding of bupivacaine and ropivacaine were considered [16]. However, since interactions with LA have been reported to occur in both the CC and SP, independent molecular docking calculations were performed for each of these sites.

Table 4. Binding site residues of each channel individualized by chains in TASK-1 (chains A and B) and K_V1.5 (chains A to D).

Channel	**Binding site residues**
TASK-1[44]	A:Q126, A:L171, A:F194, A:T198, A:T199, A:V234, A:I235, A:G236, A:F238, A:L239, A:N240, B:T93, B:M111, B:A114, B:I118
Na_V1.5[43]	L1462, I1466, F1760, Y1767
K_V1.5 (CC)[16]	A:T480, A:I508, A:V512, A:V516, B:T480, B:I508, B:V512, B:V516, C:T480, C:I508, C:V512, C:V516, D:T480, D:I508, D:V512, D:V516
K_V1.5 (SP)[16]	A:L436, A:F439, A:F440, A:I443, A:I502, A:L510, B:L436, B:F439, B:F440, B:I443, B:I502, B:L510

Regarding Na_V1.5, the analysis focused on the residues reported for lidocaine in its four domains [43]. The BS residues for each channel are shown in **Table 4**. Ultimately, ≈ 550 poses were obtained for each system, amounting to a total of 2212 poses, approximately 10 poses per ligand. This was achieved using 60 designed compounds and 5 additional compounds for validation on each of the TASK-1, Na_V1.5, and K_V1.5 channels. The compounds used for validation were the LA active against the channels, namely *R* and *S* bupivacaine, *R* and *S* ropivacaine, and lidocaine. In the case of bupivacaine and ropivacaine, the two enantiomeric forms were used, due to the relevant differences in their inhibitory activities [16,37–39,41,42,89].

Once the molecular docking results were obtained with the IFD method, binding free energy calculations were performed using the MM-GBSA method to re-score and analyze the poses obtained for each channel. The MM-GBSA method combines energy from molecular mechanics and an implicit solvation model to estimate the binding free energy of a complex. Therefore, MM-GBSA provides an intermediate level of precision and computational effort between empirical scoring methods of ligand-protein affinity and perturbation methods of free energy calculation [46].

The binding free energy is calculated as the difference between the energy of the complex, the ligand, and the protein, according to the following equation:

$$E_{binding} = E_{complex} - E_{protein} - E_{ligand} \quad (1)$$

And the change in free energy is obtained according to:

$$\Delta G_{Bind} = \Delta H - T\Delta S \approx \Delta E_{MM} + \Delta G_{Sol} - T\Delta S \quad (2)$$

Where ΔE_{MM} corresponds to $\Delta E_{internal} + \Delta E_{electrostatic} + \Delta E_{vdw}$ and $\Delta G_{Sol} = \Delta G_{GB} + \Delta G_{SA}$. The $\Delta E_{internal}$ corresponds to the bond, angle, and dihedral energies. $\Delta E_{electrostatic}$ and ΔE_{vdw} refer to electrostatic and van der Waals energies, respectively. ΔG_{GB} is the electrostatic solvation energy, which corresponds to the polar contribution, while ΔG_{SA} corresponds to the non-electrostatic solvation component that corresponds to the non-polar contribution. The Generalized Born (GB) model was used to calculate the polar contribution in this work.

Computational studies: Ranking of Poses

Due to the interest in selecting the best compounds based on two criteria: I. Best energy of MM-GBSA and II. Interaction with key binding residues, we proposed a scoring strategy to evaluate each of these criteria. After obtaining the binding free energy results, it was determined whether each pose was within a radius of 5 Å or less from any atom of the BS residues reported for the relevant LA compounds, i.e., bupivacaine and ropivacaine for TASK-1 and $K_V1.5$, and lidocaine for $Na_V1.5$. The Schrödinger python API was used to measure the distances between the residues of each protein and each ligand. To combine both criteria, the values of binding free energy and number of interactions were normalized. For the binding free energy, a value of 1 was assigned when the energy value

was more favorable (i.e., more negative values of binding free energy received higher normalization values closer to 1). For the number of interactions with key BS residues, a higher number of interactions received a normalization value closer to 1. Once the normalization values for interactions (INT_NORM) and for binding free energy (DGBIND_NORM) were established, their sum divided by two (NORMT) was calculated, and then the poses were ordered based first on the value of "INT_NORM" and then on the value of "NORMT" **(see Table S1-S4)**.

This order was assigned to give more weight to the number of interactions with the experimentally reported BS residues, and then to the binding free energy calculated with the MM-GBSA method. Consequently, only the first pose of each compound in each channel, with the best "INT_NORM" and "NORMT" values, was selected. For this resulting order, a new variable called "RANK" was assigned, wherein poses with better values received a position closer to 1 in the ranking, while the less favorable compounds had a position greater than 1.

Computational Studies: Ranking of Compounds

Once the ranking of each compound in each channel was obtained, the information was combined to identify the compounds with the best rankings across all three channels. To achieve this, the "RANK" values of each compound in each channel were added, resulting in the variable "GLOBAL RANK." Subsequently, the compounds were ordered based on their "GLOBAL RANK" values, with the first compounds being those with the lowest " GLOBAL RANK" value. Finally, the top 10 common compounds in the three channels were selected.

A schematic representation of the ranking design is shown in **Figure 2**. The ranking process for the three channels studied has been implemented in a Python library called "polypharm,"[90] which is available on GitHub: https://github.com/ucm-lbqc/polypharm. This library was designed in a versatile manner, enabling the same process to be easily adapted for other proteins of interest.

Chemistry

The reagents and solvents used in this study were purchased from Sigma-Aldrich and Merck. The reactions were monitored using thin layer chromatography (TLC) on Al TLC chromatofoils of silica GF254, which were revealed in a SPECTROLINE MODEL CM-10 camera at two wavelengths, 254 and 366 nm. Revealing solutions based on ninhydrin (for primary amines), bromocresol green (for carboxylic acids), sublimated iodine (for unsaturations), among others, were used.

Characterization of the compounds was carried out using different techniques. Infrared (IR) spectra (KBr pellets, 500–4000 cm^{-1}) were obtained using a NEXUS 670 FT-IR spectrophotometer (Thermo Nicolet, Madison, WI, USA). Nuclear magnetic resonance (NMR) spectra were recorded on a Bruker DPX 400 spectrometer (400 MHz for ^{1}H and 100 MHz for ^{13}C). Samples were dissolved in $CDCl_3$, and spectra were calibrated using tetramethylsilane (TMS) signals. Displacement (δ) and coupling constant (J) values are reported in parts per million (ppm) and Hertz (Hz), respectively. The signals were represented as follows: singlet (s), doublet (d), triplet (t), and multiplet (m). Melting points (m.p.) (uncorrected) were measured using an IA9100 m.p. electrothermal apparatus (Stone, Staffs, UK). High-resolution mass spectrometry (HRMS) spectra were obtained on

a Bruker Compact QqTOF spectrometer. The analysis was performed by direct injection using a 500 µL Hamilton syringe with a flow rate of 2 µL/min using the InfusionONE Syringe Pump NE-300. For ionization, an ESI source was used, with a voltage of 4500V, a gas temperature of 180°C, flow at 4L/min, and a nebulizer at 0.4 bar.

High-Performance Liquid Chromatography (HPLC) analysis was carried out on a YL9100 instrument with a YL9110 quaternary pump, a YL9150 autosampler, a YL9101 degassing pump, and a photodiode array (PDA) detector. Chromatogram processing was performed using Clarity software version 6.0 of 2012. A LiChroCart 125-4 LiChrospher 100 RP-18 reverse phase C-18 column (5 µM) was used. The mobile phase consisted of two solutions: the first (solution A) was a solution of 0.1% trifluoroacetic acid (TFA) in acetonitrile (CH_3CN), and solution B was an aqueous mixture of 0.1% TFA. The flow rate was 1 mL/min, and the chromatograms were acquired at a wavelength of 254 nm.

Synthesis of derivatives of bromoacetic acid (6a-f) and (*S*)-2-bromopropionic acid (7a-d).

The amidation reactions were performed using the coupling reagent *N*,*N*'-diisopropylcarbodiimide (DIC) with bromoacetic acid (**1**) or (*S*)-2-bromopropionic acid (**2**) **(Scheme 1)**. In a round-bottomed flask, a solution of bromoacetic acid (**1**) or (*S*)-2-bromopropionic acid (**2**) (1 mmol, 1 equiv.) in dichloromethane (DCM) was added at 0 °C. Then, DIC (170.33 µL, 1.1 equiv.) was added and stirred for 2 minutes for **1** or 10 minutes for **2**. Afterward, the aromatic amine (**3**) (1 mmol, 1 equiv.) was added, and the reaction was monitored using TLC. Once the reaction was complete, purification was carried out through column chromatography, and the pure amide product (**4**) was obtained.

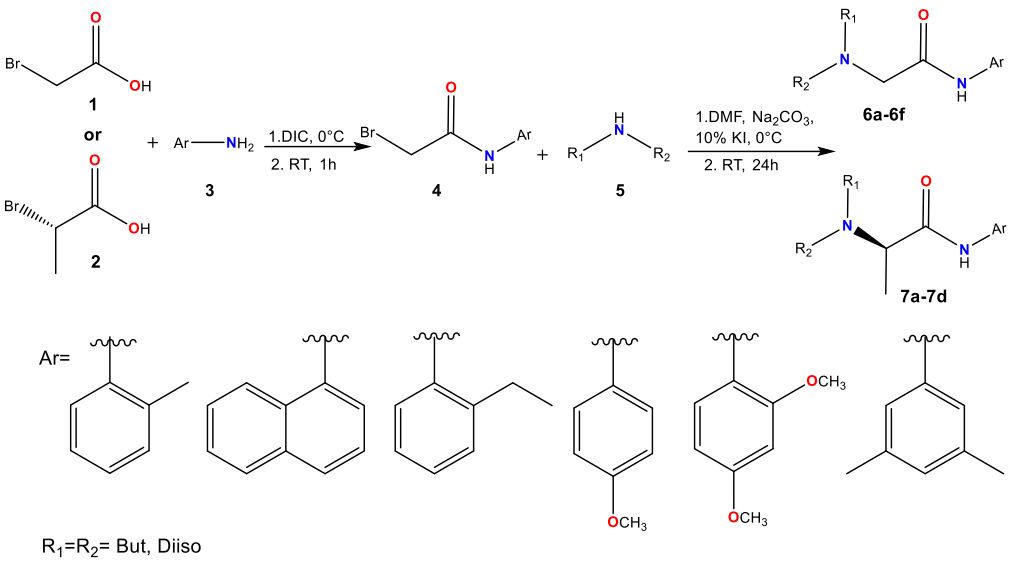

Scheme 1. Synthesis of the set of compounds 6 and 7.

In the second phase, 10 mol% potassium iodide (KI) and sodium carbonate (Na_2CO_3) (1 mmol, 1 equiv.) were dissolved in 3 mL DMF at 0 °C and added to the amide product. Subsequently, the aliphatic amine (**5**) (1.3 mmol, 1.3 equiv. for **1** or 2.3 mmol, 2.3 equiv. for **2**) dissolved in DCM was added and left stirring for 24 h at room temperature. The reaction was monitored by TLC, and the final product (**6** or **7**) was obtained. Finally, extraction with ethyl acetate (50 mL) was performed, followed by washing with water (20 mL), a saturated solution of sodium bicarbonate (20 mL), and a saturated solution of sodium chloride (20 mL). The mixture was then dried over anhydrous Na_2SO_4. The compound was purified by column chromatography using an ethyl acetate:petroleum ether mixture with a variable gradient.

2-(dibutylamine)-*N*-(*o*-tolyl)acetamide (6a)

Yellow liquid; Yield: 68.37 %; ^{1}H-NMR (400 MHz, $CDCl_3$) δ 9.41 (s, 1H), 8.15 (d, *J* = 8.1 Hz, 1H), 7.29 – 7.15 (m, 2H), 7.04 (t, *J* = 7.4 Hz, 1H), 3.20 (s, 2H), 2.57 (t, *J* = 8.1 Hz, 4H), 2.29 (s, 3H), 1.50 (m, 4H), 1.35 (m, 4H), 0.93 (t, *J* = 7.3 Hz, 6H); ^{13}C- NMR (100

MHz, $CDCl_3$) δ: 169.95 (C), 136.06 (C), 130.33 (CH), 127.00 (CH), 124.22 (CH), 121.02 (CH), 59.56 (CH_2), 55.42 (CH_2), 29.78 (CH_2), 20.58 (CH_2), 17.79 (CH_3), 13.99 (CH_3); DEPT-135 δ 130.33 (CH), 126.92 (CH), 124.22 (CH), 121.02 (CH), 59,56 (CH_2), 52.91 (CH_2), 29.78 (CH_2), 20.58 (CH_2), 17.79 (CH_3), 13.99 (CH_3); IR (KBr): υ: 3302.13, 2958.80, 2862.36, 2819.93, 1697.36, 1589.34, 1523.76, 1454.33, 752.24 cm^{-1}; HRMS (ESI, m/z): Calcd for $C_{17}H_{28}N_2O$ $[M+H]^+$ 277.2280 found 277.2278; HPLC Purity = 96.7 %; ((Solution A: (TFA 0,01 % / acetonitrilo) y (Solution B: TFA 0.01 %)), 1 mL/min, tR = 3.367 min).

2-(dibutylamine)-*N*-(2-ethylphenyl)acetamide (6b)

Yellow liquid; Yield: 72.34 %; ^{1}H-NMR (400 MHz, $CDCl_3$) δ 9.46 (s, 1H), 8.14 (d, *J* = 8.0 Hz, 1H), 7.32 – 7.18 (m, 2H), 7.11 (t, *J* = 7.4 Hz, 1H), 3.22 (s, 2H), 2.65 (m, 2H), 2.62 – 2.55 (m, 4H), 1.56 – 1.47 (m, 4H), 1.40 – 1.32 (m, 4H), 1.28 (t, *J* = 7.6 Hz, 3H), 0.94 (t, *J* = 7.3 Hz, 6H); ^{13}C-NMR (100 MHz, $CDCl_3$) δ 170.09 (C), 135.27 (C), 133.31 (C), 128.56 (CH), 126.80 (CH), 124.73 (CH), 121.45 (CH), 59.34 (CH_2), 55.39 (CH_2), 29.72 (CH_2), 24.60 (CH_2), 20.60 (CH_2), 14.24 (CH_3), 14.00 (CH_3); DEPT-135 δ 128.56 (CH), 126.80 (CH), 124.59 (CH), 121.73 (CH), 59.54 (CH_2), 55.39 (CH_2), 29.72 (CH_2), 24.44 (CH_2), 20.60 (CH_2), 14.24 (CH_3), 14,00 (CH_3); IR (KBr): υ: 3305.99, 2870.08, 2360.87, 1693.50, 1585.49, 1519.91, 1454.33, 752.24 cm^{-1}; HRMS (ESI, m/z): Calcd for $C_{18}H_{30}N_2O$ $[M+H]^+$ 291.2436 found 291.2430; HPLC Purity = 99.3 %; ((Solution A: (TFA 0.01 % / acetonitrilo) y (Solution B: TFA 0.01 %)), 1 mL/min, tR = 3.427 min).

2-(dibutylamine)-*N*-(3,5-dimethylphenyl)acetamide (6c)

Yellow liquid; Yield: 69.45 %; ^{1}H-NMR (400 MHz, $CDCl_3$) δ 9.30 (s, 1H), 7.03 (s, 2H),

6.77 (s, 1H), 3.15 (s, 2H), 2.61 – 2.52 (m, 4H), 2.33 (s, 6H), 1.53 – 1.45 (m, 4H), 1.43 – 1.31 (m, 4H), 0.95 (t, *J* = 7.3 Hz, 6H); ^{13}C-NMR (100 MHz, $CDCl_3$) δ: 169.98 (C), 138.73 (C), 137.66 (C), 125.74 (CH), 116.92 (CH), 59.41 (CH_2), 55.36 (CH_2), 29.58 (CH_2), 21.39 (CH_3), 20.62 (CH_2), 14.01 (CH_3). DEPT-135 δ 125.74 (CH), 116.92 (CH), 59.41 (CH_2), 55.36 (CH_2), 29.58 (CH_2), 21.39 (CH_3), 20.62 (CH_2), 14.01 (CH_3); IR (KBr): υ: 3294.42, 2958.80, 2862.36, 1693.50, 1612.49, 1535.34, 837.11 cm^{-1}; HRMS (ESI, m/z): Calcd for $C_{18}H_{30}N_2O$ $[M+H]^+$ 291.2436 found 291.2427; HPLC Purity = 99.5 % ((Solution A: (TFA 0.01 % / acetonitrile) y (Solution B: TFA 0.01 %))1 mL/min, tR = 3.493 min).

2-(diisopropylamine)-*N*-(3,5-dimetylphenyl)acetamide (6d)

Yellow solid; Yield: 73.65 %; m.p= 58-59 °C; ^{1}H- NMR (400 MHz, $CDCl_3$) δ 9.43 (s, 1H), 7.23 (s, 2H), 6.78 (s, 1H), 3.18 (s, 2H), 3.13 – 3.17 (m, 2H), 2.34 (s, 6H), 1.11 (d, *J* = 6.5 Hz, 12H); ^{13}C-NMR (100 MHz, $CDCl_3$) δ: 171.41 (C), 138.77 (C), 137.58 (C), 125.74 (CH), 116.89 (CH), 50.31 (CH_2, CH), 21.36 (CH_3), 20.64 (CH_3); DEPT-135 δ 125.74 (CH), 116.89 (CH), 50.32 (CH_2), 50.28 (CH), 21.36 (CH_3), 20.64 (CH_3); IR (KBr): υ: 3259.70, 2966.52, 2866.22, 2360.87, 1670.35, 1608.63, 1527.62, 775.38 cm^{-1}; HRMS (ESI, m/z): Calcd for $C_{16}H_{26}N_2O$ $[M+H]^+$ 263.2123 found 263.2120; HPLC Purity = 96.6 % ((Solution A: (TFA 0.01 % / acetonitrile) y (Solution B: TFA 0.01 %)), 1 mL/min, tR = 3.740 min).

2-(dibutylamine)-*N*-(4-methoxiphenyl)acetamide (6e)

White solid; Yield: 66.88 %; m.p= 50 - 51 °C; ^{1}H-NMR (400 MHz, $CDCl_3$) 9.27 (s, 1H), 7.48 (d, *J* = 8 Hz ,2H), 6.88 (d, *J* = 12 Hz, 2H), 3.79 (s, 3H), 3.14 (s, 2H), 2.65 – 2.43 (m, 4H), 1.53 – 1.41 (m, 4H), 1.38 – 1.24 (m, 4H), 0.93 (t, *J* = 7.3 Hz, 6H); ^{13}C- NMR (100

MHz, $CDCl_3$) δ: 169.74 (C), 156.19 (C), 131.11 (C), 120.79 (CH), 114.22 (CH), 59.27 (CH_2), 55.50 (CH_3), 55.28 (CH_2), 29.54 (CH_2), 20.61 (CH_2), 14.01 (CH_3); IR (KBr): υ: 3278.99, 2997.38, 2954.95, 2862.36 2831.50, 1666.50, 1593.20, 1527.62, 779.24 cm^{-1}; HRMS (ESI, m/z): Calcd for $C_{17}H_{28}N_2O_2$ $[M+H]^+$ 293.2229 found 293.2225; HPLC Purity = 98.2 % ((Solution A: (TFA 0.01 % / acetonitrile) y (Solution B: TFA 0.01 %)), 1 mL/min, tR = 3.393 min).

2-(dibutylamine)-*N*-(2,4-dimethoxiphenyl)acetamide (6f)

Yellow liquid; Yield: 84.04 %; ^{1}H-NMR (400 MHz, $CDCl_3$ δ 9.65 (s, 1H), 8.26 (d, *J* = 9.4 Hz, 1H), 6.42 – 6.45 (m, 2H), 3.81 (s, 3H), 3.76 (s, 3H), 3.11 (s, 2H), 2.49 (t, *J* = 7.2 Hz, 4H), 1.52 – 1.40 (m, 4H), 1.34 – 1.23 (m, 4H), 0.88 (t, *J* = 7.3 Hz, 6H); ^{13}C- NMR (100 MHz, $CDCl_3$) δ: 169.73 (C), 156.29 (C), 149.62 (C), 121.31 (C), 120.26 (CH), 103.68 (CH), 98.67 (CH), 59.82 (CH_2), 55.56 (CH_3), 55.49 (CH_3), 55.15 (CH_2), 29.67 (CH_2), 20.39 (CH_2), 14.05 (CH_3); IR (KBr): υ: 3313.71, 2870.08, 1685.79, 1600.92, 1527.62, 729.09 cm^{-1}; HRMS (ESI, m/z): Calcd for $C_{18}H_{30}N_2O_3$ $[M+H]^+$ 323.2335 found 323.2337; HPLC Purity = 98.4 % ((Solution A: (TFA 0.01 % / acetonitrilo) y (Solution B: TFA 0.01 %)), 1 mL/min, tR = 3.427 min).

2-(dibutylamine)-*N*-(4-methoxiphenyl)propanamide (7a)

Yellow liquid; Yield: 69.42 %; ^{1}H- NMR (400 MHz, $CDCl_3$) δ 9.44 (s, 1H), 7.44 (d, J = 8 Hz, 2H), 6.83 (d, *J* = 8 Hz, 2H), 3.79 (s, 3H), 3.46 (q, *J* = 7,0 Hz, 1H), 2.56 – 2.34 (m, 4H), 1.48 – 1.40 (m, 4H), 1.42 – 1.27 (m, 4H), 1.26 (d, *J* = 4.0 Hz, 3H), 0.93 (t, *J* = 7.3 Hz, 6H); ^{13}C- NMR (100 MHz, $CDCl_3$) δ: 172.57 (C), 155.95 (C), 131.52 (C), 120.48 (C), 114.20 (C), 60.08 (CH), 55.50 (CH_3), 50.55 (CH_2), 30.57 (CH_2), 20.66 (CH_2), 14.07 (CH_3), 8.33

(CH_3); IR (KBr): υ: 3313.71, 2800-3000, 1689.64, 1593.20, 1516.05, 829.39 cm^{-1}; HRMS (ESI, m/z): Calcd for $C_{18}H_{30}N_2O_2$ $[M+H]^+$ 307.2386 found 307.2379; HPLC Purity = 99.0 % ((Solution A: (TFA 0.01 % / acetonitrile) y (Solution B: TFA 0.01 %)), 1 mL/min, tR = 3.273 min).

2-(dibutylamine)-*N*-(o-tolyl)propanamide (7b)

Yellow liquid; Yield: 78.22 %; ^{1}H- NMR (400 MHz, $CDCl_3$) δ 9.52 (s, 1H), 8.15 (d, *J* = 7.9 Hz, 1H), 7.22 – 7.11 (m, 2H), 6.99 (t, *J* = 7.4 Hz, 1H), 3.48 (q, *J* = 6.6 Hz, 1H), 2.58 – 2.34 (m, 4H), 2.24 (s, 3H), 1.55 – 1.28 (m, 8H), 1.26 (d, *J* = 6.9 Hz, 3H), 0.89 (t, *J* = 8.0 Hz, 6H); ^{13}C- NMR (100 MHz, $CDCl_3$) δ: 172.83 (C), 136.45 (C), 130.29 (CH), 126.87 (CH), 126.81 (C), 123.88 (CH), 120.71 (CH), 60.58 (CH), 50.72 (CH_2), 30.81 (CH_2), 20.63 (CH_3), 17.88 (CH_3), 17.49 (CH_2), 14.00 (CH_3); DEPT-135; 130.30 (CH), 126.88 (CH), 123.88 (CH), 120.71 (CH), 60.59 (CH), 50.73 (CH_2), 30.82 (CH_2), 20.63 (CH_3), 17.89 (CH_3), 17.49 (CH_2), 14.01 (CH_3); IR (KBr): υ: 3313.71, 2958.80, 2862.36, 1697.36, 1519.91, 1454.33, 756.10 cm^{-1}; HRMS (ESI, m/z): Calcd for $C_{18}H_{30}N_2O$ $[M+H]^+$ 291.2436 found 291.2425; HPLC Purity = 96.4 % ((Solution A: (TFA 0.01 % / acetonitrile) y (Solution B: TFA 0.01 %)), 1 mL/min, tR = 3.333 min).

2-(dibutylamine)-*N*-(naphthalen-1-yl)propanamide (7c)

Yellow-orange liquid; Yield: 62.84 %; ^{1}H- NMR (400 MHz, $CDCl_3$) δ 10.26 (s, 1H), 8.26 (d, *J* = 7.5 Hz, 1H), 7.87 – 7.82 (m, 2H), 7.61 (d, *J* = 8.2 Hz, 1H), 7.53 – 7.43 (m, 3H), 3.63 (q, *J* = 6.8 Hz, 1H), 2.65 – 2.45 (m, 4H), 1,50 – 1,60 (m, 3H), 1,42 –1,33 (m, 8H), 0.90 (t, *J* = 8 Hz, 6H); ^{13}C-NMR (100 MHz, $CDCl_3$) δ: 173.07 (C), 134.09 (C), 132.93 (C), 128.88 (CH), 126.09 (CH), 125.95 (CH), 125.89 (CH), 125.77 (CH), 124.33 (CH), 120.11

(CH), 117.74 (CH), 60.76 (CH), 50.85 (CH_2), 30.74 (CH_2), 20.69 (CH_2), 14.22 (CH_3), 14.01 (CH_3); DEPT-135; 128.89 (CH), 126.10 (CH), 125.96 (CH), 125.78 (CH), 124.34 (CH), 120.11 (CH), 60.77 (CH), 50.86 (CH_2), 30.74 (CH_2), 20.70 (CH_2), 14.23 (CH_3), 14.02 (CH_3); IR (KBr): υ: 3300, 2958, 2870.08, 1697.36, 1527.62, 1492.90, 794.67 cm^{-1}; HRMS (ESI, m/z): Calcd for $C_{21}H_{30}N_2O$ $[M+H]^+$ 327.2436 found 327.2434; HPLC Purity = 100.0 % ((Solution A: (TFA 0.01 % / acetonitrile) y (Solution B: TFA 0.01 %)), 1 mL/min, tR = 3.373 min).

2-(dibutylamine)-*N*-(3,5-dimetilphenyl)propanamide (7d)

Yellow liquid; Yield: 54.92 %; ^{1}H- NMR (400 MHz, $CDCl_3$) δ 9.48 (s, 1H), 7.23 (s, 2H), 6.76 (s, 1H), 3.56 – 3.41 (m, 1H), 2.58 – 2.37 (m, 4H), 2.33 (s, 6H), 1.54 – 1.47 (m, 4H), 1.44 – 1.32 (m, 4H), 1.28 (d, *J* = 7.0 Hz, 3H), 0.96 (t, *J* = 7.3 Hz, 6H); ^{13}C- NMR (100 MHz, $CDCl_3$) δ: 172.87 (C), 138.71 (C), 137.99 (C), 125.44 (CH), 116.70 (CH), 60.20 (CH), 50.61 (CH_2), 30.57 (CH_2), 21.40 (CH_3), 20.66 (CH_2) , 14.06 (CH_3), 8.31 (CH_3); DEPT-135; 125.44, (CH) 116.70 (CH), 60.20 (CH), 50.61 (CH_2), 30.57 (CH_2), 21.40 (CH_3), 20.66 (CH_2), 14.06 (CH_3), 8.31 (CH_3); IR (KBr): υ: 3305.99, 2958.80, 2858.51, 1697.36, 1608.63, 1531.48, 837.11 cm^{-1}; HRMS (ESI, m/z): Calcd for $C_{19}H_{32}N_2O$ $[M+H]^+$ 305.2593 found 305.2594; HPLC Purity = 98.7 % ((Solution A: (TFA 0.01 % / acetonitrile) y (Solution B: TFA 0.01 %)), 1 mL/min, tR = 3.663 min).

Biological activity

Oocyte preparation and channel cloning

To obtain *X. laevis* oocytes, the frogs were anesthetized with 2 g/L of tricaine methanesulfonate, and the ovarian lobes were mechanically separated with forceps. The

oocytes were incubated for 120 minutes in an OR2 solution containing in mM: NaCl 82.5, KCl 2, $MgCl_2$ 1, HEPES 5 (pH 7.5) supplemented with 2 mg/mL of collagenase II (Sigma) to remove residual connective tissue and obtain individual oocytes. Subsequently, the oocytes were washed with a ND96 solution containing in mM: NaCl 96, KCl 2, $CaCl_2$ 1.8, $MgCl_2$ 1, HEPES 5 (pH 7.5, adjusted with NaOH) and stored at 18 °C in ND96 solution supplemented with 1 mL of gentamicin (50 mg/L), sodium pyruvate (275 mg/L) and (90 mg/L) theophylline (inhibits further oocyte maturation) before and after RNA injection.

In order to overexpress the channel in the oocyte, each of the channels to be measured was subcloned (complementary DNA (cDNA); human TASK-1 (KCNK3, NM_002246), h K_V1.5 (KCNA5, NM_002234), h Na_V1.5 (hH1, M77235), TASK-4/TALK-2 (KCNK17, NM_AF358910), TREK-1 (KCNK2, AF004711) and K_{ir}2.1 (KCNJ2, NM_017296) into pSGEM, pBF1 or pSP64 expression vector, and the cDNA was linearized with NheI or MluI. Complementary RNA (cRNA) was synthesized with the mMESSAGE mMACHINE-Kit (Ambion). The quality of the cRNA was tested on an agarose gel by electrophoresis. cRNA was quantified using a UV-Vis spectrophotometer (NanoDrop 2000). Subsequently, the channel was transfected in the oocytes in stages IV and V, for which 50 nL (TASK-1, K_V1.5 or TREK-1), 10 ng (Na_V1.5 or TASK-4) o 2.5 ng (K_{ir}2.1) per oocyte of cRNA was injected with a NanojectII microinjector (Drummond Scientific). The oocytes were stored in 24-well plates for 24 to 48 h at 18 °C. After this time, the overexpression of each channel was monitored through electrophysiology.

Two-electrode Voltage-Clamp Recordings

Two-electrode voltage clamp measurements were performed 24 or 48 hours after cRNA

injection at room temperature (20 - 22 °C) in ND96 recording solution with a TurboTEC-10CD (npi) amplifier and a Digidata 1550B (for TASK-1 and $K_V1.5$) and 1440A (for $Na_V1.5$) A/D converter from Axon Instruments. Micropipettes were fabricated from GB 150TF-8P borosilicate glass capillaries (Science Products) elongated in a DMZ-Universal Puller (Zeitz, Germany). Recording pipettes, had a resistance of 0.3 - 0.8 MΩ (for $K_V1.5$ and TASK-1) or 0.2 - 1.0 MΩ (for $Na_V1.5$), when filled with a 3M KCl solution. ND96 was used as bath solution. Data acquisition was performed using Clampex 10 software (Axon Instruments), and data were analyzed with ClampFit 10 (Axon Instruments) and Origin 7 (Origin Lab Corporation).

For compound inhibition testing, from a holding potential of -80 mV a first test pulse to 0 mV of 1 s duration was followed by a repolarization step at -80 mV for 1 s, directly followed by another 1 s test pulse at +40 mV. The sweep time interval was 10 s for $K_V1.5$ and TASK-1 channels. For the $Na_V1.5$ channel, the block was analyzed with voltage steps from a holding potential of −80 mV. A first depolarizing pulse to −30 mV of 50 ms duration was applied, followed by a 5 ms step to -80 mV. The sweep time interval was 10 s. The compounds were evaluated at different concentrations, and the IC_{50} (half-maximal inhibitory concentration) was determined.

Preparation of compounds and determination of IC_{50}.

All compounds were prepared and stored in aliquots dissolved in DMSO on the day of the experiment. The solutions were prepared using ND96 solution as the solvent, according to the required concentration. The mean half-maximum inhibitory concentration (IC_{50}) was determined from Hill plots using six concentrations, n=6 (for TASK-1, $K_V1.5$, and

$Na_V1.5$), and are expressed as mean ± SEM coming from the different replicate measurements (n = 6 - 15 replicates).

Statistical analysis

To analyze statistically the TEVC results, the system (protein) and the drugs were selected as factors. The independent and combined effects of the factors on the response variable (inhibition percentage) were evaluated using generalized linear models (GLMs) and Heteroscedastic tests. Statistical analysis of Figure 4, 5 and 7, was performed using R software version 4.3.2 [91]. It was verified if the data followed a normal distribution [92], then it was verified if variances were homogeneous [93], and according to this result, GLM with Gamma or Gaussian distribution using identity as the link function (figure 4 and 5) [94] was used. To evaluate the effect of the factors on the data behavior was performed ANOVA [95] in every GLM, and according to the results, multiple comparisons were performed using a post hoc analysis with the Tukey test. For figure 7, Welch´s Heteroscedastic F test [95] was employed, and multiple comparisons were performed using the Bonferroni test [96,97]. The significance level (alpha) for all tests was 0.05, and the codes for the significance levels are shown as follows: ***p < 0.001, **p < 0.01, *p < 0.05.

Cardiomyocyte Assays

Ethics statement

A total of 10 patients with sinus rhythm (SR) (N=5) or atrial fibrillation (AF) (N=5) undergoing open heart surgery for coronary artery bypass grafting, heart valve replacement

or heart transplantation were included in the study (**Table S7**). A written informed consent was given by all patients. The study protocol involving human tissue samples was approved by the responsible Ethics Committee of the Medical Faculty of Heidelberg University (Germany; S-017/2013) and was conducted in accordance with the 1964 Declaration of Helsinki.

Cardiomyocyte isolation

The right atrial human tissue samples were transported in chilled Ca^{2+}-free solution (100 mM NaCl, 10 mM KCl, 1.2 mM KH_2PO_4, 5 mM $MgSO_4$, 50 mM taurine, 5 mM 3-(*N*-morpholino)propanesulfonic acid (MOPS), 30 mM 2,3-butanedione monoxime and 20 mM glucose, pH 7.0 with NaOH). After dissection into small chunks, the samples were rinsed for five minutes with calcium-free Tyrode's solution, which was oxygenated with 100 % O_2 at 37 °C. The samples were then digested with collagenase type I (288 U/mL; Worthington) and protease type XXIV (5 mg/mL; Sigma-Aldrich, Steinheim, Germany) for 10-15 minutes, followed by an increase in calcium concentration to 0.2 mM. After an additional 35 minutes of agitation in protease-free solution, rod-shaped single cardiomyocytes were harvested. The suspension was centrifuged, and the cells were resuspended in storage ("Kraftbrühe", KB) medium (20 mM KCl, 10 mM KH_2PO_4, 25 mM glucose, 40 mM D-Mannitol, 70 mM K glutamate, 10 mM β-hydroxybutyrate, 20 mM taurine, 10 mM ethylene glycol tetraacetic acid (EGTA), and 1 % albumin) until usage in patch-clamp experiments.

Patch Clamp Electrophysiology

Patch-clamp glass pipettes were fabricated from borosilicate glass (1B120F-4; World

Precision Instruments, Berlin, Germany). After back-filling with patch-clamp internal solution (134 mM K gluconate, 6 mM NaCl, 1.2 mM $MgCl_2$, 1 mM Mg-ATP, 10 mM HEPES, pH 7.2 with KOH), tip resistances ranged from 5 to 10 MΩ. All experiments were carried out at room temperature under constant superfusion with patch-clamp extracellular solution containing 137 mM NaCl, 5.4 mM KCl, 1 mM $MgCl_2$, 2 mM $CaCl_2$, 10 mM HEPES, 10 mM glucose (pH 7.3 with NaOH). AP-recordings were performed in current clamp mode: The holding current was adjusted such that the cell's resting membrane potential was approximately -70 mV at baseline. APs were induced by short (5 ms) depolarizing current pulses at a rate of 0.5 Hz. Data was not adjusted for potential differences caused by liquid junctions, and no leak subtraction was performed.

Statistical Analysis

Data acquisition and analysis were performed using the pCLAMP10 software (Axon Instruments) and statistical analysis was done using Prism 8 (GraphPad Software, La Jolla, CA, USA). Data is presented as the mean ± standard error of the mean (SEM). Statistical comparisons were made using one-way ANOVA. A p-value of < 0.05 was considered significant.

In-silico Trials for the Pharmacological Management of AF with Compound 6f

The efficacy of compound **6f** for both acute AF cardioversion and long-term AF prevention was assessed in a population of 45 virtual-atria human models with variability in ionic current channel densities.

Population of Atrial Cardiomyocyte Models

To capture human variability in ionic currents, a population of atrial cardiomyocyte models

was generated. The population was constructed with a modified version of the CRN model [98] as in Wiedmann *et al.*, 2020, to include K_{2P} channel family. The family comprises the Tandem of P domains as a weak inward rectifying K^+ channel (TWIK)-related acid-sensitive K^+ channel (TASK-1, $K_{2P}3.1$; Wiedmann *et al.*, 2020). To account for variability, the ionic current densities of the modified CRN model were varied up to ± 50% [100]. This variation included the ultrarapid and rapid delayed-rectifier K^+ current (G_{Kur}, G_{Kr}), transient outward (G_{to}) and inward rectifier K^+ current (G_{K1}), L-type Ca^{2+} current (G_{CaL}), fast Na^+ current (G_{Na}), Na^+/K^+ pump (G_{NaK}), and the K_{2P} current (G_{K2P}) densities. A hundred myocyte models, generated with Latin Hypercube sampling, were calibrated against experimental data obtained from patients in sinus rhythm and AF [101]. A calibrated sample of 45 atrial cardiomyocyte models was used to populate a whole-atria model.

Populations of virtual-atria models

Whole-atria simulations were performed using a mean bi-atrial model derived from averaging the atrial anatomy of 47 human subjects [102]. A population of 45 virtual-atria models was generated by assigning the single-cell properties of each atrial cardiomyocyte model to the left atrial tissue and scaling them by reported regional differences in ion channel expression to the right atrium, crista terminalis, pectinate muscles, left atrial appendage, and atrio-ventricular rings [103,104]. Regional heterogeneities in conduction velocity and anisotropy ratio were likewise considered, setting the longitudinal velocity in the bulk tissue to 80 cm/s.

AF inducibility

AF was induced in the virtual-atria models by imposing spiral wave re-entries as the initial conditions of the simulation. AF dynamics were then analyzed for 7 s of activity [105]. The three-dimensional monodomain equation of the transmembrane voltage was solved using the MonoAlg3D software [106].

In-silico drug trials

Sustained (>7 s) AF episodes were subjected to the virtual administration of three concentrations (i.e., 1, 10, and 100 μM) of compound **6f**. Efficacy for acute AF cardioversion was investigated by applying each concentration 2 s after AF induction, and the episode was recorded for another 5 s. AF was considered successfully cardioverted by the drug if the atria were free of arrhythmic activity no later than 7 s after AF induction [105].

Long-term AF prevention was modeled by repeating the AF initiation protocol after drug application [103]. Drug action was simulated using simple pore-block models based on the 50% inhibitory concentration and Hill coefficient profiles. The ionic current block of each concentration according to the inhibitory curves presented in **Figure 6** is summarized in **Table 5**.

Table 5. Corresponding ionic current block based on the inhibition curves for I_{K2P} (TASK-1), I_{Kur} ($K_V1.5$) and I_{Na} ($Na_V1.5$).

Drug	Concentration	Ionic current block (%)		
		I_{Kur}	I_{Na}	I_{K2P}
Compound 6f	1 μM	0	16	58
	10 μM	2.5	30	75
	100 μM	50	65	85

Determination of ADME Properties

The SwissADME website, a freely available online tool [72], was utilized to evaluate the ADME properties (absorption, distribution, metabolism, and excretion) of the synthesized compounds and LA. This involved the calculation of gastrointestinal absorption, pharmacokinetic descriptors, and physicochemical descriptors, including the assessment of compliance with the Lipinski's Rule of Five [73,107,108]

Hemocytotoxicity assay

To evaluate cytotoxicity, the hemolysis of the compounds with the best simultaneous blocking activity on the channels (**6e, 6f, 7a, 7b** and **7c**) was considered, modifying the protocol of Chen 2018[109]. Thus, non-heparinized human blood was collected. Erythrocytes were washed three times in 1X PBS (phosphate-buffered saline: NaCl, 8 g/L; KCl, 0.2 g/L; Na_2HPO_4, 1.44 g/L; and KH_2PO_4, 0.24 g/L; pH 7.4) and then used to prepare a 3% red blood cell (RBC) suspension. The assay was performed in a 96-well polypropylene microplate.

The compounds were prepared from 200 mM stock solutions in DMSO. Subsequently, 1:2 serial dilutions were made in 1X PBS, with final concentrations from 400 to 0.2 µM to a final volume of 200 µL per well. The microplate was incubated for 2 h at 37 °C and centrifuged at 3400 rpm for 5 minutes. Finally, 100 µL of the supernatant was transferred and measured in a 96-well plate. Hemoglobin release was monitored by photometric analysis of the supernatant at 540 nm using an Epoch™ Microplate Spectrophotometer (BioTek® Instruments, Inc. Winooski, Vermont 05404-0998 USA).

A 3% RBC suspension treated with Tween 20 was used to obtain total lysis as a positive control. The negative control was a suspension of GR with PBS. Each experiment was performed in triplicate at all concentrations used. The percentage of hemolysis was calculated with the following equation (1), where Ad: absorbance of the dilution, A0: absorbance of the blank (RBC suspension with PBS) and At: total absorbance (positive control).

$$\% \text{ hemolysis} = \frac{Ad - A0}{At - A0} x\ 100 \qquad (1)$$

Data availability

Data supporting the original contributions presented in the study are included in the article and supplementary materials.

ASSOCIATED CONTENT

Support Information

Author contributions

L.C-A[†], M.B., A.D. and M.P. contributed equally to this work.

The manuscript was written with contributions of all authors. All authors approved the final version of the manuscript.

Funding and additional information

The authors acknowledge the Research Group of the Laboratory of Organic Synthesis and Biological Activity, Laboratory of Electrophysiology of the Institute of Physiology and Pathophysiology, Philipps University. Marburg, Germany and the Center for Bioinformatics, Simulation and Modelling (CBSM) of the University of Talca, Fondecyt

Project 1200531 and 1230446. L.C-A. acknowledges the ANID National Doctorate Scholarship 2019 Folio N° 21190020. M.B. acknowledges FONDECYT-ANID for his postdoctoral grant Nº 3210774. P.P-M. acknowledges the ANID National Doctorate Scholarship 2019 Folio N° 21190245. PA.C-A. acknowledges the ANID National Doctorate Scholarship 2021 Folio N° 21220448. CS was funded in part by research grants from the German Heart Foundation /German Foundation of Heart Research (F/03/19, Atrial fibrillation grant), the Else-Kröner Fresenius Foundation (EKFS Clinician-Scientist professorship), the German Centre for Cardiovascular Research (DZHK TRP grant, innovation cluster grant, shared expertise). CS ad FW are members of the CRC1425 and CRC1550, funded by the German Research Foundation (#422681845 and #464424253).

Conflict of interest

The authors declare that they have no conflicts of interest with the contents of this article.

Notes: ChatGPT (OpenAI, 2022) was used to proofread and enhance the grammatical accuracy of the manuscript.

References

[1] D. Calvo, D. Filgueiras-Rama, J. Jalife, Mechanisms and drug development in atrial fibrillation, Pharmacol. Rev. 70 (2018) 505–525. https://doi.org/10.1124/pr.117.014183.

[2] S.M. Schumacher, D.P. McEwen, L. Zhang, K.L. Arendt, K.M. Van Genderen, J.R. Martens, Antiarrhythmic drug-induced internalization of the atrial-specific K+ channel Kv1.5, Circ. Res. 104 (2009) 1390–1398. https://doi.org/10.1161/CIRCRESAHA.108.192773.

[3] M.K. Chung, L.L. Eckhardt, L.Y. Chen, H.M. Ahmed, R. Gopinathannair, J.A. Joglar, P.A. Noseworthy, Q.R. Pack, P. Sanders, K.M. Trulock, Lifestyle and Risk Factor Modification for Reduction of Atrial Fibrillation: A Scientific Statement From the American Heart Association, Circulation. 141 (2020) E750–E772. https://doi.org/10.1161/CIR.0000000000000748.

[4] L.J. Young, S. Antwi-Boasiako, J. Ferrall, L.E. Wold, P.J. Mohler, M. El Refaey, Genetic and non-genetic risk factors associated with atrial fibrillation, Life Sci. 299 (2022). https://doi.org/10.1016/J.LFS.2022.120529.

[5] D. Conen, Epidemiology of atrial fibrillation, Eur. Heart J. 39 (2018) 1323–1324. https://doi.org/10.1093/EURHEARTJ/EHY171.

[6] S. Nattel, M. Harada, Atrial Remodeling and Atrial Fibrillation: Recent Advances

and Translational Perspectives, J. Am. Coll. Cardiol. 63 (2014) 2335–2345. https://doi.org/10.1016/J.JACC.2014.02.555.
[7] J. Heijman, N. Voigt, S. Nattel, D. Dobrev, Cellular and Molecular Electrophysiology of Atrial Fibrillation Initiation, Maintenance, and Progression, Circ. Res. 114 (2014) 1483–1499. https://doi.org/10.1161/CIRCRESAHA.114.302226.
[8] U. Ravens, C. Poulet, E. Wettwer, M. Knaut, Atrial selectivity of antiarrhythmic drugs., J. Physiol. 591 (2013) 4087–97. https://doi.org/10.1113/jphysiol.2013.256115.
[9] U. Ravens, E. Wettwer, Ultra-rapid delayed rectifier channels: Molecular basis and therapeutic implications, Cardiovasc. Res. 89 (2011) 776–785. https://doi.org/10.1093/cvr/cvq398.
[10] C. Antzelevitch, A. Burashnikov, Atrial-selective sodium channel block as a novel strategy for the management of atrial fibrillation, J. Electrocardiol. 42 (2009) 543–548. https://doi.org/10.1016/J.JELECTROCARD.2009.07.007.
[11] J.R. Ehrlich, P. Biliczki, S.H. Hohnloser, S. Nattel, Atrial-Selective Approaches for the Treatment of Atrial Fibrillation, J. Am. Coll. Cardiol. 51 (2008) 787–792. https://doi.org/10.1016/J.JACC.2007.08.067.
[12] J.R. Ehrlich, S. Nattel, Novel Approaches for Pharmacological Management of Atrial Fibrillation, Drugs 2009 697. 69 (2012) 757–774. https://doi.org/10.2165/00003495-200969070-00001.
[13] U. Ravens, Antiarrhythmic therapy in atrial fibrillation, Pharmacol. Ther. 128 (2010) 129–145. https://doi.org/10.1016/J.PHARMTHERA.2010.06.004.
[14] J.W. Ford, J.T. Milnes, New drugs targeting the cardiac ultra-rapid delayed-rectifier current (I Kur): rationale, pharmacology and evidence for potential therapeutic value, J. Cardiovasc. Pharmacol. 52 (2008) 105–120. https://doi.org/10.1097/FJC.0B013E3181719B0C.
[15] J.Z. YEH, C.M. ARMSTRONG, Immobilisation of gating charge by a substance that simulates inactivation, Nature. 273 (1978) 387–389. https://doi.org/10.1038/273387a0.
[16] A.K. Kiper, M. Bedoya, S. Stalke, S. Marzian, D. Ramírez, A. de la Cruz, D.A. Peraza, A. Vera-Zambrano, J.C.E.M. Montesinos, B.A.A. Ramos, S. Rinné, T. Gonzalez, C. Valenzuela, W. Gonzalez, N. Decher, Identification of a critical binding site for local anaesthetics in the side pockets of Kv1 channels, Br. J. Pharmacol. 178 (2021) 3034–3048. https://doi.org/10.1111/BPH.15480.
[17] S. Marzian, P.J. Stansfeld, M. Rapedius, S. Rinné, E. Nematian-Ardestani, J.L. Abbruzzese, K. Steinmeyer, M.S.P. Sansom, M.C. Sanguinetti, T. Baukrowitz, N. Decher, Side pockets provide the basis for a new mechanism of Kv channel-specific inhibition, Nat. Chem. Biol. 9 (2013) 507–513. https://doi.org/10.1038/nchembio.1271.
[18] S.H. Limberg, M.F. Netter, C. Rolfes, S. Rinné, G. Schlichthörl, M. Zuzarte, T. Vassiliou, R. Moosdorf, H. Wulf, J. Daut, F.B. Sachse, N. Decher, TASK-1 channels may modulate action potential duration of human atrial cardiomyocytes., Cell. Physiol. Biochem. 28 (2011) 613–24. https://doi.org/10.1159/000335757.
[19] C. Schmidt, F. Wiedmann, N. Voigt, X.B. Zhou, J. Heijman, S. Lang, V. Albert, S. Kallenberger, A. Ruhparwar, G. Szabó, K. Kallenbach, M. Karck, M. Borggrefe, P. Biliczki, J.R. Ehrlich, I. Baczkó, P. Lugenbiel, P.A. Schweizer, B.C. Donner, H.A. Katus, D. Dobrev, D. Thomas, Upregulation of K2P 3.1 K + Current Causes Action Potential Shortening in Patients with Chronic Atrial Fibrillation, Circulation. 132 (2015) 82–92. https://doi.org/10.1161/CIRCULATIONAHA.114.012657.

[20] C. Schmidt, F. Wiedmann, X.B. Zhou, J. Heijman, N. Voigt, A. Ratte, S. Lang, S.M. Kallenberger, C. Campana, A. Weymann, R. De Simone, G. Szabo, A. Ruhparwar, K. Kallenbach, M. Karck, J.R. Ehrlich, I. Baczkó, M. Borggrefe, U. Ravens, D. Dobrev, H.A. Katus, D. Thomas, Inverse remodelling of K2P3.1 K+ channel expression and action potential duration in left ventricular dysfunction and atrial fibrillation: implications for patient-specific antiarrhythmic drug therapy, Eur. Heart J. 38 (2017) 1764–1774. https://doi.org/10.1093/EURHEARTJ/EHW559.

[21] A.S. Barth, S. Merk, E. Arnoldi, L. Zwermann, P. Kloos, M. Gebauer, K. Steinmeyer, M. Bleich, S. Kääb, M. Hinterseer, H. Kartmann, E. Kreuzer, M. Dugas, G. Steinbeck, M. Nabauer, Reprogramming of the human atrial transcriptome in permanent atrial fibrillation: Expression of a ventricular-like genomic signature, Circ. Res. 96 (2005) 1022–1029. https://doi.org/10.1161/01.RES.0000165480.82737.33.

[22] C. Schmidt, F. Wiedmann, C. Beyersdorf, Z. Zhao, I. El-Battrawy, H. Lan, G. Szabo, X. Li, S. Lang, S. Korkmaz-Icöz, K. Rapti, A. Jungmann, A. Ratte, O.J. Müller, M. Karck, G. Seemann, I. Akin, M. Borggrefe, X.B. Zhou, H.A. Katus, D. Thomas, Genetic Ablation of TASK-1 (Tandem of P Domains in a Weak Inward Rectifying K+ Channel-Related Acid-Sensitive K+ Channel-1) (K2P3.1) K+ Channels Suppresses Atrial Fibrillation and Prevents Electrical Remodeling, Circ. Arrhythmia Electrophysiol. 12 (2019). https://doi.org/10.1161/CIRCEP.119.007465/FORMAT/EPUB.

[23] J. Kisselbach, C. Seyler, P.A. Schweizer, R. Gerstberger, R. Becker, H.A. Katus, D. Thomas, Modulation of K2P 2.1 and K2P 10.1 K(+) channel sensitivity to carvedilol by alternative mRNA translation initiation., Br. J. Pharmacol. 171 (2014) 5182–94. https://doi.org/10.1111/bph.12596.

[24] M. Kraft, A. Büscher, F. Wiedmann, Y. L'hoste, W.E. Haefeli, N. Frey, H.A. Katus, C. Schmidt, Current Drug Treatment Strategies for Atrial Fibrillation and TASK-1 Inhibition as an Emerging Novel Therapy Option, Front. Pharmacol. 12 (2021) 191. https://doi.org/10.3389/FPHAR.2021.638445/BIBTEX.

[25] F. Wiedmann, C. Schmidt, Novel drug therapies for atrial fibrillation, Nat. Rev. Cardiol. 21 (2024) 275–276. https://doi.org/10.1038/s41569-024-01004-2.

[26] A.K. Kiper, S. Rinné, C. Rolfes, D. Ramírez, G. Seebohm, M.F. Netter, W. González, N. Decher, Kv1.5 blockers preferentially inhibit TASK-1 channels: TASK-1 as a target against atrial fibrillation and obstructive sleep apnea?, Pflugers Arch. Eur. J. Physiol. 467 (2015) 1081–1090. https://doi.org/10.1007/s00424-014-1665-1.

[27] W.A. Catterall, Voltage-gated sodium channels at 60: Structure, function and pathophysiology, J. Physiol. 590 (2012) 2577–2589. https://doi.org/10.1113/jphysiol.2011.224204.

[28] D. Jiang, H. Shi, L. Tonggu, T.M. Gamal El-Din, M.J. Lenaeus, Y. Zhao, C. Yoshioka, N. Zheng, W.A. Catterall, Structure of the Cardiac Sodium Channel, Cell. 180 (2020) 122-134.e10. https://doi.org/10.1016/j.cell.2019.11.041.

[29] M. O'Reilly, L.C. Sommerfeld, C. O'Shea, S. Broadway-Stringer, S. Andaleeb, J.S. Reyat, S.N. Kabir, D. Stastny, A. Malinova, D. Delbue, L. Fortmueller, K. Gehmlich, D. Pavlovic, B. V Skryabin, A.P. Holmes, P. Kirchhof, L. Fabritz, Familial atrial fibrillation mutation M1875T-SCN5A increases early sodium current and dampens the effect of flecainide, EP Eur. 25 (2023) 1152–1161. https://doi.org/10.1093/europace/euac218.

[30] A. Burashnikov, J.M. Di Diego, A.C. Zygmunt, L. Belardinelli, C. Antzelevitch, Atrium-selective sodium channel block as a strategy for suppression of atrial

fibrillation: differences in sodium channel inactivation between atria and ventricles and the role of ranolazine, Circulation. 116 (2007) 1449–1457. https://doi.org/10.1161/CIRCULATIONAHA.107.704890.
[31] H.M. King, Gregory S, Goyal Amandeep, Grigorova Y, Antiarrhythmic Medications., In: StatPe, StatPearls Publishing, 2023. https://pubmed.ncbi.nlm.nih.gov/29493947/.
[32] M. Aguilar, F. Xiong, X.Y. Qi, P. Comtois, S. Nattel, Potassium Channel Blockade Enhances Atrial Fibrillation-Selective Antiarrhythmic Effects of Optimized State-Dependent Sodium Channel Blockade, Circulation. 132 (2015) 2203–2211. https://doi.org/10.1161/CIRCULATIONAHA.115.018016.
[33] H. Ni, D.G. Whittaker, W. Wang, W.R. Giles, S.M. Narayan, H. Zhang, Synergistic anti-arrhythmic effects in human atria with combined use of sodium blockers and acacetin, Front. Physiol. 8 (2017) 946. https://doi.org/10.3389/FPHYS.2017.00946/FULL.
[34] M. Aguilar-Shardonofsky, E.J. Vigmond, S. Nattel, P. Comtois, In Silico Optimization of Atrial Fibrillation-Selective Sodium Channel Blocker Pharmacodynamics, Biophys. J. 102 (2012) 951–960. https://doi.org/10.1016/J.BPJ.2012.01.032.
[35] H.A. Fozzard, M.F. Sheets, D.A. Hanck, M. Chahine, M.E. O, The sodium channel as a target for local anesthetic drugs, (2011). https://doi.org/10.3389/fphar.2011.00068.
[36] D. V. Kalinin, V.I. Pantsurkin, B.Y. Syropyatov, S.A. Kalinina, I.P. Rudakova, M.I. Vakhrin, A. V. Dolzhenko, Synthesis, local anaesthetic and antiarrhythmic activities of N-alkyl derivatives of proline anilides, Eur. J. Med. Chem. 63 (2013) 144–150. https://doi.org/10.1016/j.ejmech.2013.02.003.
[37] C. Arias, M. Guizy, M. David, S. Marzian, T. González, N. Decher, C. Valenzuela, Kvβ1.3 reduces the degree of stereoselective bupivacaine block of Kv1.5 channels, Anesthesiology. 107 (2007) 641–651. https://doi.org/10.1097/01.anes.0000282100.32923.5c.
[38] M. Longobardo, E. Delpón, R. Caballero, J. Tamargo, C. Valenzuela, Structural determinants of potency and stereoselective block of hKv1.5 channels induced by local anesthetics, Mol. Pharmacol. 54 (1998) 162–169. https://doi.org/10.1124/mol.54.1.162.
[39] G. Du, X. Chen, M.S. Todorovic, S. Shu, J. Kapur, D.A. Bayliss, TASK channel deletion reduces sensitivity to local anesthetic-induced seizures, Anesthesiology. 115 (2011) 1003–1011. https://doi.org/10.1097/ALN.0b013e3182343660.
[40] H. Zhang, H. Ji, Z. Liu, Y. Ji, X. You, G. Ding, Z. Cheng, Voltage-dependent blockade by bupivacaine of cardiac sodium channels expressed in Xenopus oocytes, Neurosci. Bull. 30 (2014) 697–710. https://doi.org/10.1007/s12264-013-1449-1.
[41] A.P. Schwoerer, H. Scheel, P. Friederich, A comparative analysis of bupivacaine and ropivacaine effects on human cardiac SCN5A channels, Anesth. Analg. 120 (2015) 1226–1234. https://doi.org/10.1213/ANE.0000000000000646.
[42] T. Elajnaf, D.T. Baptista-Hon, T.G. Hales, Potent inactivation-dependent inhibition of adult and neonatal NaV1.5 channels by lidocaine and levobupivacaine, Anesth. Analg. 127 (2018) 650–660. https://doi.org/10.1213/ANE.0000000000003597.
[43] P.T. Nguyen, K.R. DeMarco, I. Vorobyov, C.E. Clancy, V. Yarov-Yarovoy, Structural basis for antiarrhythmic drug interactions with the human cardiac sodium channel, Proc. Natl. Acad. Sci. U. S. A. 116 (2019) 2945–2954. https://doi.org/10.1073/pnas.1817446116.
[44] S. Rinné, A.K. Kiper, K.S. Vowinkel, D. Ramírez, M. Schewe, M. Bedoya, D. Aser,

I. Gensler, M.F. Netter, P.J. Stansfeld, T. Baukrowitz, W. Gonzalez, N. Decher, The molecular basis for an allosteric inhibition of K+-flux gating in K2P channels, Elife. 8 (2019). https://doi.org/10.7554/eLife.39476.

[45] W. Sherman, T. Day, M.P. Jacobson, R.A. Friesner, R. Farid, Novel procedure for modeling ligand/receptor induced fit effects, J. Med. Chem. 49 (2006) 534–553. https://doi.org/10.1021/jm050540c.

[46] S. Genheden, U. Ryde, The MM/PBSA and MM/GBSA methods to estimate ligand-binding affinities, Expert Opin. Drug Discov. 10 (2015) 449. https://doi.org/10.1517/17460441.2015.1032936.

[47] J.R. Dunetz, J. Magano, G.A. Weisenburger, Large-Scale Applications of Amide Coupling Reagents for the Synthesis of Pharmaceuticals, Org. Process Res. Dev. 20 (2016) 140–177. https://doi.org/10.1021/op500305s.

[48] A. Williams, I.T. Ibrahim, Carbodiimide Chemistry: Recent Advances, 1981. https://pubs.acs.org/sharingguidelines (accessed December 30, 2020).

[49] V.R. Pattabiraman, J.W. Bode, Rethinking amide bond synthesis, Nature. 480 (2011) 471–479. https://doi.org/10.1038/nature10702.

[50] P.W. Seavill, J.D. Wilden, The preparation and applications of amides using electrosynthesis, Green Chem. 22 (2020) 7737–7759. https://doi.org/10.1039/d0gc02976a.

[51] C.H. Kindler, C.S. Yost, A.T. Gray, Local anesthetic inhibition of baseline potassium channels with two pore domains in tandem, Anesthesiology. 90 (1999) 1092–1102. https://doi.org/10.1097/00000542-199904000-00024.

[52] J. Miake, E. Marbán, H.B. Nuss, Functional role of inward rectifier current in heart probed by Kir2.1 overexpression and dominant-negative suppression., Undefined. 111 (2003) 1529–1536. https://doi.org/10.1172/JCI17959.

[53] D.J. Beuckelmann, M. Näbauer, E. Erdmann, Alterations of K+ currents in isolated human ventricular myocytes from patients with terminal heart failure, Circ. Res. 73 (1993) 379–385. https://doi.org/10.1161/01.RES.73.2.379.

[54] D. Dobrev, E. Graf, E. Wettwer, H.M. Himmel, O. Hála, C. Doerfel, T. Christ, S. Schüler, U. Ravens, Molecular Basis of Downregulation of G-Protein–Coupled Inward Rectifying K + Current (I K,ACh) in Chronic Human Atrial Fibrillation, Circulation. 104 (2001) 2551–2557. https://doi.org/10.1161/hc4601.099466.

[55] F. Wiedmann, S. Rinné, B. Donner, N. Decher, H.A. Katus, C. Schmidt, Mechanosensitive TREK-1 two-pore-domain potassium (K2P) channels in the cardiovascular system, Prog. Biophys. Mol. Biol. 159 (2021) 126–135. https://doi.org/10.1016/J.PBIOMOLBIO.2020.05.007.

[56] W. Wang, M. Zhang, P. Li, H. Yuan, N. Feng, Y. Peng, L. Wang, X. Wang, An increased TREK-1-like potassium current in ventricular myocytes during rat cardiac hypertrophy, J. Cardiovasc. Pharmacol. 61 (2013) 302–310. https://doi.org/10.1097/FJC.0B013E318280C5A9.

[57] C. Terrenoire, I. Lauritzen, F. Lesage, G. Romey, M. Lazdunski, A TREK-1–Like Potassium Channel in Atrial Cells Inhibited by β-Adrenergic Stimulation and Activated by Volatile Anesthetics, Circ. Res. 89 (2001) 336–342. https://doi.org/10.1161/HH1601.094979.

[58] F. Wiedmann, J.S. Schulte, B. Gomes, M.P. Zafeiriou, A. Ratte, F. Rathjens, E. Fehrmann, B. Scholz, N. Voigt, F.U. Müller, D. Thomas, H.A. Katus, C. Schmidt, Atrial fibrillation and heart failure-associated remodeling of two-pore-domain potassium (K2P) channels in murine disease models: focus on TASK-1, Basic Res. Cardiol. 113 (2018) 1–14. https://doi.org/10.1007/S00395-018-0687-9/FIGURES/5.

[59] S.D. Unudurthi, X. Wu, L. Qian, F. Amari, B. Onal, N. Li, M.A. Makara, S.A. Smith, J. Snyder, V. V. Fedorov, V. Coppola, M.E. Anderson, P.J. Mohler, T.J. Hund, Two-Pore K+ channel TREK-1 regulates sinoatrial node membrane excitability, J. Am. Heart Assoc. 5 (2016). https://doi.org/10.1161/JAHA.115.002865.

[60] C. Schmidt, F. Wiedmann, P.A. Schweizer, R. Becker, H.A. Katus, D. Thomas, Novel electrophysiological properties of dronedarone: inhibition of human cardiac two-pore-domain potassium (K2P) channels, Naunyn. Schmiedebergs. Arch. Pharmacol. 385 (2012) 1003–1016. https://doi.org/10.1007/s00210-012-0780-9.

[61] A. Ratte, F. Wiedmann, M. Kraft, H.A. Katus, C. Schmidt, Antiarrhythmic properties of ranolazine: Inhibition of atrial fibrillation associated TASK-1 potassium channels, Front. Pharmacol. 10 (2019) 1367. https://doi.org/10.3389/FPHAR.2019.01367/BIBTEX.

[62] T.K. Nayak, S. Harinath, S. Nama, K. Somasundaram, S.K. Sikdar, Inhibition of human two-pore domain K+ channel TREK1 by local anesthetic lidocaine: Negative cooperativity and half-of-sites saturation kinetics, Mol. Pharmacol. 76 (2009) 903–917. https://doi.org/10.1124/MOL.109.056838.

[63] K. Staudacher, I. Staudacher, E. Ficker, C. Seyler, J. Gierten, J. Kisselbach, A.K. Rahm, K. Trappe, P.A. Schweizer, R. Becker, H.A. Katus, D. Thomas, Carvedilol targets human K 2P3.1 (TASK1) K + leak channels, Br. J. Pharmacol. 163 (2011) 1099–1110. https://doi.org/10.1111/j.1476-5381.2011.01319.x.

[64] C. Schmidt, F. Wiedmann, P.A. Schweizer, R. Becker, H.A. Katus, D. Thomas, Class I antiarrhythmic drugs inhibit human cardiac two-pore-domain K(+) (K2 $_2$p) channels., Eur. J. Pharmacol. 721 (2013) 237–248. https://doi.org/10.1016/J.EJPHAR.2013.09.029.

[65] C. Schmidt, F. Wiedmann, S.M. Kallenberger, A. Ratte, J.S. Schulte, B. Scholz, F.U. Müller, N. Voigt, M.P. Zafeiriou, J.R. Ehrlich, U. Tochtermann, G. Veres, A. Ruhparwar, M. Karck, H.A. Katus, D. Thomas, Stretch-activated two-pore-domain (K2P) potassium channels in the heart: Focus on atrial fibrillation and heart failure, Prog. Biophys. Mol. Biol. 130 (2017) 233–243. https://doi.org/10.1016/J.PBIOMOLBIO.2017.05.004.

[66] I. Staudacher, C. Illg, S. Chai, I. Deschenes, S. Seehausen, D. Gramlich, M.E. Müller, T. Wieder, A.K. Rahm, C. Mayer, P.A. Schweizer, H.A. Katus, D. Thomas, Cardiovascular pharmacology of K 2P 17.1 (TASK-4, TALK-2) two-pore-domain K + channels, Naunyn. Schmiedebergs. Arch. Pharmacol. 391 (2018) 1119–1131. https://doi.org/10.1007/S00210-018-1535-Z.

[67] C. Seyler, P.A. Schweizer, E. Zitron, H.A. Katus, D. Thomas, Vernakalant activates human cardiac K2P17.1 background K+ channels, Biochem. Biophys. Res. Commun. 451 (2014) 415–420. https://doi.org/10.1016/j.bbrc.2014.07.133.

[68] A. Paasche, F. Wiedmann, M. Kraft, F. Seibertz, V. Herlt, P.L. Blochberger, N. Jávorszky, M. Beck, L. Weirauch, T. Seeger, A. Blank, W.E. Haefeli, R. Arif, A.L. Meyer, G. Warnecke, M. Karck, N. Voigt, N. Frey, C. Schmidt, Acute antiarrhythmic effects of SGLT2 inhibitors–dapagliflozin lowers the excitability of atrial cardiomyocytes, Basic Res. Cardiol. 119 (2024) 93–112. https://doi.org/10.1007/s00395-023-01022-0.

[69] E. Wettwer, T. Christ, S. Endig, N. Rozmaritsa, K. Matschke, J.J. Lynch, M. Pourrier, J.K. Gibson, D. Fedida, M. Knaut, U. Ravens, The new antiarrhythmic drug vernakalant: ex vivo study of human atrial tissue from sinus rhythm and chronic atrial fibrillation, Cardiovasc. Res. 98 (2013) 145–154. https://doi.org/10.1093/cvr/cvt006.

[70] J. Eldstrom, Z. Wang, H. Xu, M. Pourrier, A. Ezrin, K. Gibson, D. Fedida, The Molecular Basis of High-Affinity Binding of the Antiarrhythmic Compound Vernakalant (RSD1235) to Kv1.5 Channels, Mol. Pharmacol. 72 (2007) 1522–1534. https://doi.org/10.1124/mol.107.039388.
[71] C. Seyler, J. Li, P.A. Schweizer, H.A. Katus, D. Thomas, Inhibition of cardiac two-pore-domain K+ (K2P) channels by the antiarrhythmic drug vernakalant – Comparison with flecainide, Eur. J. Pharmacol. 724 (2014) 51–57. https://doi.org/10.1016/j.ejphar.2013.12.030.
[72] A. Daina, O. Michielin, V. Zoete, SwissADME: a free web tool to evaluate pharmacokinetics, drug-likeness and medicinal chemistry friendliness of small molecules, Sci. Reports 2017 71. 7 (2017) 1–13. https://doi.org/10.1038/srep42717.
[73] C.A. Lipinski, F. Lombardo, B.W. Dominy, P.J. Feeney, Experimental and computational approaches to estimate solubility and permeability in drug discovery and development settings, 46 (2001) 3–26.
[74] F. Montanari, G.F. Ecker, Prediction of drug–ABC-transporter interaction — Recent advances and future challenges, Adv. Drug Deliv. Rev. 86 (2015) 17–26. https://doi.org/10.1016/J.ADDR.2015.03.001.
[75] B. Testa, S.D. Krämer, The biochemistry of drug metabolism - An introduction part 2. Redox reactions and their enzymes, Chem. Biodivers. 4 (2007) 257–405. https://doi.org/10.1002/CBDV.200790032.
[76] V.S. de Sena Pereira, C.B. Silva de Oliveira, F. Fumagalli, F. da Silva Emery, N.B. da Silva, V.F. de Andrade-Neto, Cytotoxicity, hemolysis and in vivo acute toxicity of 2-hydroxy-3-anilino-1,4-naphthoquinone derivatives, Toxicol. Reports. 3 (2016) 756–762. https://doi.org/10.1016/j.toxrep.2016.09.007.
[77] D.S. Ragsdale, J.C. McPhee, T. Scheuer, W.A. Catterall, Molecular determinants of state-dependent block of Na+ channels by local anesthetics, Science (80-.). 265 (1994) 1724–1728. https://doi.org/10.1126/science.8085162.
[78] D.S. Ragsdale, J.C. McPhee, T. Scheuer, W.A. Catterall, Common molecular determinants of local anesthetic, antiarrhythmic, and anticonvulsant block of voltage-gated Na+ channels., Proc. Natl. Acad. Sci. 93 (1996) 9270–9275. https://doi.org/10.1073/pnas.93.17.9270.
[79] M.J. Kornet, A.P. Thio, Oxindole-3-spiropyrrolidines and -piperidines. Synthesis and local anesthetic activity, J. Med. Chem. 19 (1976) 892–898. https://doi.org/10.1021/jm00229a007.
[80] T.J. Colatsky, C.H. Follmer, Potassium channels as targets for antiarrhythmic drug action, Drug Dev. Res. 19 (1990) 129–140. https://doi.org/10.1002/ddr.430190204.
[81] B.I. Khodorov, Sodium inactivation and drug-induced immobilization of the gating charge in nerve membrane, Prog. Biophys. Mol. Biol. 37 (1981) 49–89. https://doi.org/10.1016/0079-6107(82)90020-7.
[82] J.C. Shelley, A. Cholleti, L.L. Frye, J.R. Greenwood, M.R. Timlin, M. Uchimaya, Epik: A software program for pKa prediction and protonation state generation for drug-like molecules, J. Comput. Aided. Mol. Des. 21 (2007) 681–691. https://doi.org/10.1007/S10822-007-9133-Z.
[83] M.R. Hestenes, E. Stiefel, Methods of conjugate gradients for solving linear systems, J. Res. Natl. Bur. Stand. (1934). 49 (1952) 409. https://doi.org/10.6028/jres.049.044.
[84] K.E.J. Rödström, A.K. Kiper, W. Zhang, S. Rinné, A.C.W. Pike, M. Goldstein, L.J. Conrad, M. Delbeck, M.G. Hahn, H. Meier, M. Platzk, A. Quigley, D. Speedman, L. Shrestha, S.M.M. Mukhopadhyay, N.A. Burgess-Brown, S.J. Tucker, T. Müller, N. Decher, E.P. Carpenter, A lower X-gate in TASK channels traps inhibitors within

the vestibule, Nature. 582 (2020) 443–447. https://doi.org/10.1038/s41586-020-2250-8.
[85] Z. Li, X. Jin, T. Wu, G. Huang, K. Wu, J. Lei, X. Pan, N. Yan, Structural Basis for Pore Blockade of the Human Cardiac Sodium Channel Nav1.5 by the Antiarrhythmic Drug Quinidine, Angew. Chemie Int. Ed. 60 (2021) 11474–11480. https://doi.org/10.1002/ANIE.202102196.
[86] Y. Mazola, J.C.E. Márquez Montesinos, D. Ramírez, L. Zúñiga, N. Decher, U. Ravens, V. Yarov-Yarovoy, W. González, Common Structural Pattern for Flecainide Binding in Atrial-Selective Kv1.5 and Nav1.5 Channels: A Computational Approach, Pharmaceutics. 14 (2022) 1356. https://doi.org/10.3390/pharmaceutics14071356.
[87] G. Madhavi Sastry, M. Adzhigirey, T. Day, R. Annabhimoju, W. Sherman, Protein and ligand preparation: parameters, protocols, and influence on virtual screening enrichments, J. Comput. Aided. Mol. Des. 27 (2013) 221–234. https://doi.org/10.1007/s10822-013-9644-8.
[88] M.H.M. Olsson, C.R. Søndergaard, M. Rostkowski, J.H. Jensen, PROPKA3: Consistent Treatment of Internal and Surface Residues in Empirical p K a Predictions, J. Chem. Theory Comput. 7 (2011) 525–537. https://doi.org/10.1021/ct100578z.
[89] C. Valenzuela, E. Delpón, M.M. Tamkun, J. Tamargo, D.J. Snyders, Stereoselective block of a human cardiac potassium channel (Kv1.5) by bupivacaine enantiomers, Biophys. J. 69 (1995) 418–427. https://doi.org/10.1016/S0006-3495(95)79914-3.
[90] F. Adasme, M. Bedoya, ucm-lbqc/polypharm: Polypharm v0.4.3, (2024). https://doi.org/10.5281/zenodo.11123342.
[91] R Core Team, R: A Language and Environment for Statistical Computing, (2018).
[92] S.S. SHAPIRO, M.B. WILK, An analysis of variance test for normality (complete samples), Biometrika. 52 (1965) 591–611. https://doi.org/10.1093/biomet/52.3-4.591.
[93] M.B. Brown, A.B. Forsythe, Robust Tests for the Equality of Variances, J. Am. Stat. Assoc. 69 (1974) 364. https://doi.org/10.2307/2285659.
[94] G.K. Smyth, Generalized Linear Models with Varying Dispersion, J. R. Stat. Soc. Ser. B. 51 (1989) 47–60. https://doi.org/10.1111/j.2517-6161.1989.tb01747.x.
[95] O. Dag, A. Dolgun, N.M. Konar, Onewaytests: An R package for one-way tests in independent groups designs, R J. 10 (2018) 175–199. https://doi.org/10.32614/RJ-2018-022.
[96] C.E. Bonferroni, Teoria statistica delle classi e calcolo, Seeber. (1936) 1–62.
[97] H. Abdi, The Bonferonni and Šidák Corrections for Multiple Comparisons, Encycl. Meas. Stat. 3 (2007).
[98] M. Courtemanche, R.J. Ramirez, S. Nattel, Ionic mechanisms underlying human atrial action potential properties: insights from a mathematical model, Am. J. Physiol. Circ. Physiol. 275 (1998) H301–H321. https://doi.org/10.1152/ajpheart.1998.275.1.H301.
[99] F. Wiedmann, C. Beyersdorf, X. Zhou, A. Büscher, M. Kraft, J. Nietfeld, T.P. Walz, L.A. Unger, A. Loewe, B. Schmack, A. Ruhparwar, M. Karck, D. Thomas, M. Borggrefe, G. Seemann, H.A. Katus, C. Schmidt, Pharmacologic twik-related acid-sensitive k+ channel (Task-1) potassium channel inhibitor a293 facilitates acute cardioversion of paroxysmal atrial fibrillation in a porcine large animal model, J. Am. Heart Assoc. 9 (2020) 1–16. https://doi.org/10.1161/JAHA.119.015751.
[100] A. Muszkiewicz, X. Liu, A. Bueno-Orovio, B.A.J. Lawson, K. Burrage, B. Casadei, B. Rodriguez, From ionic to cellular variability in human atrial myocytes: An

integrative computational and experimental study, Am. J. Physiol. - Hear. Circ. Physiol. 314 (2018) H895–H916. https://doi.org/10.1152/ajpheart.00477.2017.
[101] C. Sánchez, A. Bueno-Orovio, E. Wettwer, S. Loose, J. Simon, U. Ravens, E. Pueyo, B. Rodriguez, Inter-subject variability in human atrial action potential in sinus rhythm versus chronic atrial fibrillation, PLoS One. 9 (2014). https://doi.org/10.1371/journal.pone.0105897.
[102] C. Nagel, S. Schuler, O. Dössel, A. Loewe, A bi-atrial statistical shape model for large-scale in silico studies of human atria: Model development and application to ECG simulations, Med. Image Anal. 74 (2021) 102210. https://doi.org/10.1016/j.media.2021.102210.
[103] A. Dasí, A. Roy, R. Sachetto, J. Camps, A. Bueno-Orovio, B. Rodriguez, In-silico drug trials for precision medicine in atrial fibrillation: From ionic mechanisms to electrocardiogram-based predictions in structurally-healthy human atria , Front. Physiol. . 13 (2022).
[104] C. Sánchez, A. Bueno-Orovio, E. Pueyo, B. Rodríguez, Atrial fibrillation dynamics and ionic block effects in six Heterogeneous human 3D virtual atria with distinct repolarization dynamics, Front. Bioeng. Biotechnol. 5 (2017) 1–13. https://doi.org/10.3389/fbioe.2017.00029.
[105] E. Matene, V. Jacquemet, Fully automated initiation of simulated episodes of atrial arrhythmias, Europace. 14 (2012) 17–24. https://doi.org/10.1093/europace/eus271.
[106] R. Sachetto Oliveira, B. Martins Rocha, D. Burgarelli, W. Meira, C. Constantinides, R. Weber dos Santos, Performance evaluation of GPU parallelization, space-time adaptive algorithms, and their combination for simulating cardiac electrophysiology, Int. j. Numer. Method. Biomed. Eng. 34 (2018) 1–17. https://doi.org/10.1002/cnm.2913.
[107] A. Daina, O. Michielin, V. Zoete, ILOGP: A simple, robust, and efficient description of n-octanol/water partition coefficient for drug design using the GB/SA approach, J. Chem. Inf. Model. 54 (2014) 3284–3301. https://doi.org/10.1021/CI500467K/SUPPL_FILE/CI500467K_SI_001.PDF.
[108] M. Hay, D.W. Thomas, J.L. Craighead, C. Economides, J. Rosenthal, Clinical development success rates for investigational drugs, Nat. Biotechnol. 2014 321. 32 (2014) 40–51. https://doi.org/10.1038/nbt.2786.
[109] Z. Chen, H. Duan, X. Tong, P. Hsu, L. Han, S.L. Morris-Natschke, S. Yang, W. Liu, K.-H. Lee, Cytotoxicity, Hemolytic Toxicity, and Mechanism of Action of Pulsatilla Saponin D and Its Synthetic Derivatives, J. Nat. Prod. 81 (2018) 465–474. https://doi.org/10.1021/acs.jnatprod.7b00578.

TOC Graphic